fractal and fractional

MDPI

Article

Numerical Solutions of Variable-Coefficient Fractional-in-Space KdV Equation with the Caputo Fractional Derivative

Che Han and Yu-Lan Wang *

Department of Mathematics, Inner Mongolia University of Technology, Hohhot 010051, China; hanche0905@163.com

* Correspondence: wylnei@163.com; Tel.: +86-0471-657-5470

Abstract: In this paper, numerical solutions of the variable-coefficient Korteweg-De Vries (vcKdV) equation with space described by the Caputo fractional derivative operator is developed. The propagation and interaction of vcKdV equation in different cases, such as breather soliton and periodic suppression soliton, are numerically simulated. Especially, the Fourier spectral method is used to solve the fractional-in-space vcKdV equation with breather soliton. From numerical simulations and compared with other methods, it can be easily seen that our method has low computational complexity and higher precision.

Keywords: fractional-in-space different equation; variable-coefficient KdV equation; numerical simulations; Fourier spectral method

Citation: Han, C.; Wang, Y.-L. Numerical Solutions of Variable-Coefficient Fractional-in-Space KdV Equation with the Caputo Fractional Derivative. *Fractal Fract.* **2022**, *6*, 207. https://doi.org/10.3390/fractalfract6040207

Academic Editor: Omar Bazighifan

Received: 11 March 2022
Accepted: 30 March 2022
Published: 7 April 2022

1. Introduction

The KdV equation is one of the most notable integrable equations and has found numerous applications in many fields of science, such as plasma physics, nonlinear optics, telecommunications, fluid mechanics, condensed matter physics and dust plasma. The KdV equation was derived by Korteweg and de Vires in 1895 [1]. There are many analytical methods to obtain the analytical solutions of the KdV equation, including Hirota method, Darboux transformation and so on [2,3]. The symmetry method is used to solve many fractional differential equations, such as the seventh-order generalized KdV equation [4], the generalized KdV-Burgers-Kuramoto equation [5] and the time fractional generalized fifth-order KdV equation [6]. Qin [7] used the Hirota method to obtain the N-soliton solutions of the coupled KdV-mKdV system based on Bell polynomials. Chen [8] used the test function method combined with the bilinear to obtain the lump solutions to the generalized variable coefficient Burgers equation.

There are also many good numerical methods to solve the KdV equation. Yan [9] used a local discontinuous Galerkin method to solve the KdV equation. Jackaman [10] advanced the design of the conservative finite element discretizations for the vectorial modified KdV equation. Energy-conserving Hamiltonian boundary value methods were used to solve the KdV equation by Brugnano [11]. However, the numerical method that can be applied to solve the space fractional vcKdV equation with breather soliton and periodic suppression soliton is seldom researched. Therefore, a Fourier spectral method is developed in this paper which has low computational complexity and higher precision. We consider the KdV equation with the following form:

$$v_t + \alpha_1 v^2 D_x^{\beta_1} v + \varepsilon v D_x^{\beta_2} v + \alpha_2 v_{xxx} + \alpha_3 v_x = 0, \tag{1}$$

equipped with the following initial and boundary conditions,

$$\begin{cases} v(x,0) = v_0, \quad a \le x \le b, \\ v(a,t) = v(b,t) = 0, \end{cases} \tag{2}$$

where $D_x^{\beta_1} v$, $D_x^{\beta_2} vs.$ denote Caputo fractional derivative operator which has the following form,

$$D_x^{\beta} v(x) = \begin{cases} \frac{1}{\Gamma(1-\beta_1)} \int_0^x (x-\tau)^{-\beta_1} \frac{\partial v(\tau)}{\partial \tau} d\tau, & 0 < \beta_1 < 1, \\ \frac{\partial v(x)}{\partial x}, & \beta_1 = 1, \end{cases} \tag{3}$$

and ε, α_1, α_2, α_3 are positive parameters.

When $\alpha_1 = \alpha_3 = \alpha_4 = \beta_1 = 0$, $\alpha_2 = \mu$ and $\beta_2 = 1$, Equation (1) becomes the KdV equation,

$$v_t + \varepsilon v v_x + \mu v_{xxx} = 0. \tag{4}$$

When $\varepsilon = \frac{3}{2}$, $\alpha_1 = 0$, $\alpha_2 = \frac{1}{6}$, $\alpha_3 = -\omega_0$, $\beta_1 = 0$ and $\beta_2 = 1$, Equation (1) is reduced to the gKdV equation [12],

$$v_t - \omega_0 v_x + \tfrac{3}{2} v v_x + \tfrac{1}{6} v_{xxx} = 0. \tag{5}$$

When $\varepsilon = \alpha_3 = \alpha_4 = 0$ and $\beta_1 = 1$, Equation (1) becomes the modified KdV(mKdV) equation,

$$v_t + \alpha_1 v^2 v_x + \alpha_2 v_{xxx} = 0, \tag{6}$$

which has important applications in studying nonlinear optics [13,14], and quantum mechanics [15].

When $\varepsilon = \varepsilon(t)$, $\beta_2 = 1$, $\alpha_1 = \alpha_1(t)$, $\beta_1 = 1$, $\alpha_2 = \alpha_2(t)$, $\alpha_3 = \alpha_3(t)$ and $\alpha_1(t)\alpha_2(t) \neq 0$, Equation (1) becomes the generalized variable-coefficient KdV-modified KdV equation [16],

$$v_t + \varepsilon(t) v v_x + \alpha_1(t) v^2 v_x + \alpha_2(t) v_{xxx} + \alpha_3(t) v_x = 0. \tag{7}$$

Consulting materials in the literature, we discover that the numerical solutions of the space fractional vcKdV equation are rarely researched. Therefore, some numerical solutions of the vcKdV equation are given in this manuscript. From the numerical simulations and compared with other methods, it can be easily seen that our method has low computational complexity and higher precision.

This paper is organized as follows: In Section 2, we introduce the numerical method. Many numerical experiments are provided in Section 3. Section 4 concludes the paper.

2. Numerical Approximation Method

We use the Fourier spectral method [17–19] for spatial discretization. In order to standardize the space period $[a, b]$ to $[0, 2\pi]$, we use the transformations $x \to \frac{2\pi(x-a)}{L}$ and $L = b - a$. v is converted into a Fourier space with respect to x. We use Fast Fourier transform [20] to complete this operation. We use Fourier transform for Equation (1) in spatial domain,

$$\begin{cases} \frac{\partial \hat{v}}{\partial t} = -\varepsilon \mathcal{F}[v \mathcal{F}^{-1}((ik)^{\beta_2} \hat{v})] - \alpha_1 \mathcal{F}[v^2 \mathcal{F}^{-1}((ik)^{\beta_1} \hat{v})] - \alpha_2 (ik)^3 \hat{v} - \alpha_3 (ik\hat{v}), \\ \hat{v}(k, 0) = \hat{v}_0, \end{cases} \tag{8}$$

Let $x_j = j\Delta x = \frac{2\pi L j}{N}$, $N > 0$ and N is an integer, $L = b - a$, $j = 0, 1, \cdots\cdots, N-1$. We use the discrete Fourier transform for v,

$$\hat{v}(k, t) = \mathcal{F}(v) = \frac{1}{N} \sum_{j=1}^{N-1} v(x_j, t) e^{-ikx_j}, \quad -\frac{N}{2} \leq k \leq \frac{N}{2} - 1, \tag{9}$$

and the inverse formula is

$$v(x_j,t)=\mathcal{F}^{-1}(\hat{v})=\sum_{k=-\frac{N}{2}}^{\frac{N}{2}-1}\hat{v}(k,t)e^{ikx_j},\quad 0\le j\le N-1. \tag{10}$$

Next, the fourth-order Runge–Kutta method is used to solve the ordinary differential Equation (8),

$$\begin{cases} k_1=r(t_n,\hat{v}_n),\\ k_2=r(t_n+\frac{\tau}{2},\hat{v}_n+\frac{\tau k_1}{2}),\\ k_3=r(t_n+\frac{\tau}{2},\hat{v}_n+\frac{\tau k_2}{2}),\\ k_4=r(t_n+\tau,\hat{v}_n+\tau k_3),\\ \hat{v}_{n+1}=\hat{v}_n+\frac{\tau}{6}(k_1+2k_2+2k_3+k_4), \end{cases} \tag{11}$$

where τ is step-size and $r(t,\hat{v})=-\varepsilon\mathcal{F}[v\mathcal{F}^{-1}((ik)^{\beta_2}\hat{v})]-\alpha_1\mathcal{F}[v^2\mathcal{F}^{-1}((ik)^{\beta_1}\hat{v})]-\alpha_2(ik)^3\hat{v}-\alpha_3(ik\hat{v})$.

We mark

$$\begin{cases} V=(\hat{v}_0(k,t),\hat{v}_1(k,t),\cdots,\hat{v}_{N-1}(k,t))^T,\\ R(t,V)=(r_0(t,\hat{v}_0(t)),r_1(t,\hat{v}_0(t)),\cdots,r_{N-1}(t,\hat{v}_{N-1}(t)))^T,\\ V_0(k)=(\hat{v}_{00}(k),\hat{v}_{01}(k),\cdots,\hat{v}_{0(N-1)}(k))^T, \end{cases} \tag{12}$$

where $n=1,\cdots,\frac{T}{\tau}$.

Equation (8) can be reduced to

$$\begin{cases} \frac{\partial V}{\partial t}=R(t,V),\\ V(k,0)=V_0. \end{cases} \tag{13}$$

Then, we can obtain the solving formula [21]

$$\begin{cases} k_{j1}=r_j(t_n,\hat{v}_{0,n},\hat{v}_{1,n},\cdots,\hat{v}_{N-1,n}),\\ k_{j2}=r_j(t_n+\frac{h}{2},\hat{v}_{0,n}+\frac{hk_{01}}{2},\cdots,\hat{v}_{N-1,n}+\frac{hk_{(N-1)1}}{2}),\\ k_{j3}=r_j(t_n+\frac{h}{2},\hat{v}_{0,n}+\frac{hk_{02}}{2},\cdots,\hat{v}_{N-1,n}+\frac{hk_{(N-1)2}}{2}),\\ k_{j4}=r_j(t_n+h,\hat{v}_{0,n}+hk_{03},\cdots,\hat{v}_{N-1,n}+hk_{(N-1)3}),\\ \hat{v}_{j,n+1}=\hat{v}_{j,n}+\frac{h}{6}(k_{j1}+2k_{j2}+2k_{j3}+k_{j4}), \end{cases} \tag{14}$$

where $j=0,1,\cdots,N-1$.

Definition 1. *A class of the single-step method for solving an ordinary differential equation in the form of:*

$$V_{n+1}=V_n+h\phi(V_n,t_n,h), \tag{15}$$

where incremental function ϕ is determined by $R(t,V)$, that is a function of V_n, t_n, τ.

Theorem 1. *If $\phi(V,t,\tau)$ satisfies the Lipschitz condition in V, then the numerical method that is given by Equation (15) is stable.*

Proof. We refer the reader to [22–24] for the details of the proof. □

Lemma 1. *Let $e_n=V_n-V(t_n)$ and D is constant [22]. If $\|e_{n+1}\|\le(1+\tau L)\|e_n\|+D$, then*

$$\|e_n\|\le\frac{D(1+\tau L)^n}{\tau L}+(1+\tau L)^n\|e_0\|\le\frac{D}{\tau L}-(e^{LT}-1)+e^{LT}\|e_0\|. \tag{16}$$

Theorem 2. *If $\phi(V,t,\tau)$ is a continuous function in V, t, τ, which satisfies the Lipschitz condition on $0 \le \tau \le \tau_0$, $0 \le t \le T$, $-\infty \le v_i \le \infty$, then Equation (15) is convergent [22].*

Theorem 3. *Let $V(t_n)$ be the analytical solution of problem (13) and V_n is the numerical solution. If $\phi(V,t,\tau)$ satisfies the Lipschitz condition on $0 \le \tau \le \tau_0$, $0 \le t \le T$ and Equation (15) is the fourth-order method, then the error estimate has the following form*

$$|e_n| \le e^{LT}(|e_0| + cT\tau^4 + L\tau M_0), \tag{17}$$

where $M_0 = max(|e_0|, |e_1|, \cdots, |e_{n-1}|)$ and L is lipschitz constant.

Proof. If Equation (15) is the fourth-order one-step method, then $V(t)$ satisfies

$$V(t_{n+1}) = V(t_n) + \tau\phi(t_n, V(t_n), \tau) + \boldsymbol{O}(\tau^5). \tag{18}$$

By denoting $e_n = V(t_n) - V_n$, we have

$$|e_{n+1}| - |e_n| \le |e_{n+1} - e_n| = \left|\tau(\phi(t_n, V(t_n), \tau) - \phi(t_n, V_n, \tau)) + \boldsymbol{o}(\tau^5)\right| \le \tau L|e_n| + \boldsymbol{O}(\tau^5). \tag{19}$$

Summing over n, we get

$$|e_n| - |e_0| \le \tau L \sum_{k=0}^{n-1} |e_k| + nc\tau^5, \tag{20}$$

$$|e_n| \le \tau L \sum_{k=0}^{n-1} |e_k| + cT\tau^4 + |e_0|. \tag{21}$$

Using the Gronwall inequality, we have

$$|e_n| \le e^{LT}(|e_0| + cT\tau^4 + L\tau M_0). \tag{22}$$

□

Finally, we find the numerical solution using the inverse discrete Fourier transform [25].

3. Simulation Results

Numerical solutions of the space fractional vcKdV equation are obtained in this chapter. We use the error norms, L_2, L_∞ and GRE (global relative error) to test the accuracy of the method: $L_2 = \sqrt{\frac{1}{N}\sum_{j=1}^{N}[v(x_j,t) - v^*(x_j,t)]^2}$, $L_\infty = \max\limits_{1\le j\le N} \mid v(x_j,t) - v^*(x_j,t) \mid$, GRE $= \frac{\sum_{j=1}^{N}|v(x_j,t)-v^*(x_j,t)|}{\sum_{j=1}^{N}|v^*(x_j,t)|}$, where $v(x_j,t)$ and $v^*(x_j,t)$ are the numerical solution and analytical solution. The order of convergence in space is computed by

$$order = \frac{\log \frac{\|v_N(x,t)-v^*(x,t)\|}{\|v_{\frac{N}{2}}(x,t)-v^*(x,t)\|}}{\log 2}. \tag{23}$$

Example 1. *Let $\varepsilon = 1$, $\beta_2 = 1$ and $\alpha_1 = \alpha_3 = \alpha_4 = \beta_1 = 0$ in Equation (1). The initial value is as follows,*

$$v(x,0) = 3c(sech^2((kx - x_0)), \tag{24}$$

with

$$k = \frac{1}{2}\sqrt{\frac{c}{\alpha_2}}, \quad \omega = ck, \tag{25}$$

where c, x_0 are constant parameters.

Referring to the numerical experiment in [26–30], the analytical solution is as follows:

$$v^*(x,t) = 3c(sech^2((kx - \omega t - x_0)), \quad -2 \le x \le 2. \tag{26}$$

In this simulation, we set $\alpha_2 = 4.84 \times 10^{-4}$, $c = 0.5$, $x_0 = 6$, $\tau = 0.01$ and $N = 512$. By present method, the numerical results are given in Table 1. Tables 2 and 3 show the absolute error by our numerical method, Hybrid method [26], B-spline method [27], ANS method [29], HBI method [30] at $t = 0.005, 0.01$. Then, we shall investigate the space fractional KdV equation. Table 4 shows comparison of L_∞ at different β_2. For the space fractional KdV equation, we take (26) as reference solution because the analytical solution can not be obtained. Figures 1 and 2 show the logarithm of absolute errors by present method, Hybrid numerical method [26], B-spline method [27], ANS method [29], HBI method [30] at the the selected notes for $t = 0.005, 0.01$, which shows that our numerical method has higher accuracy than other methods. Comparisons are made between numerical solutions and analytical solutions at $t = 0, 1, 2$ in Figure 3. Figure 4 presents absolute error at $x = 2$. Numerical solutions at $t = 1, 2$ and $\beta_2 = 0.9, 0.99, 1$ are plotted in Figures 5 and 6. Numerical solutions at different β_2 are presented in Figure 7.

Table 1. Spatial numerical errors L_∞, L_2 and their corresponding convergence rates at $t = 0.001$ for Example 1.

N	L_∞	*Order*	L_2	*Order*
32	7.3429×10^{-4}	–	4.1640×10^{-4}	–
64	6.9269×10^{-4}	$N^{-0.0842}$	2.4502×10^{-4}	$N^{-0.7651}$
128	2.6108×10^{-5}	$N^{-4.7297}$	8.3098×10^{-6}	$N^{-4.8819}$
256	1.1068×10^{-9}	$N^{-14.5257}$	3.8198×10^{-10}	$N^{-14.4090}$
512	1.0904×10^{-10}	$N^{-3.3436}$	3.2646×10^{-11}	$N^{-3.5486}$

Table 2. Comparison of absolute errors at $t = 0.005$.

x	Absolute Error				
	HBI [30]	**ANS [29]**	**Hybrid [26]**	**B–Spline [27]**	**Present Method**
0.1	9.7700×10^{-6}	2.0000×10^{-8}	1.5900×10^{-6}	1.1900×10^{-6}	8.0000×10^{-8}
0.5	6.7880×10^{-3}	5.2021×10^{-4}	4.8032×10^{-4}	6.5700×10^{-5}	1.0000×10^{-8}
0.6	5.8627×10^{-3}	4.9210×10^{-5}	1.1316×10^{-4}	1.8600×10^{-5}	1.9000×10^{-7}
0.7	5.9116×10^{-4}	3.6400×10^{-6}	1.3030×10^{-5}	1.6500×10^{-6}	1.0000×10^{-8}
0.8	4.9840×10^{-5}	6.4000×10^{-7}	1.4100×10^{-6}	1.3000×10^{-7}	1.0000×10^{-8}
0.9	4.1400×10^{-6}	5.0000×10^{-8}	1.2000×10^{-7}	1.0000×10^{-8}	1.0000×10^{-8}
1.0	3.5000×10^{-7}	1.0000×10^{-8}	1.0000×10^{-8}	0.0000	1.0000×10^{-8}

Table 3. Comparison of absolute errors at $t = 0.01$.

x	Absolute Error				
	HBI [30]	**ANS [29]**	**Hybrid [26]**	**B–Spline [27]**	**Present Method**
0.2	2.3064×10^{-4}	1.7400×10^{-6}	5.0200×10^{-6}	7.2000×10^{-7}	8.0000×10^{-8}
0.5	1.3048×10^{-2}	9.8242×10^{-4}	8.9174×10^{-4}	1.1370×10^{-4}	6.0000×10^{-8}
0.6	1.1900×10^{-2}	5.5860×10^{-5}	2.3296×10^{-4}	3.5900×10^{-5}	1.9000×10^{-7}
0.7	1.2044×10^{-3}	7.4500×10^{-6}	2.5860×10^{-5}	4.0100×10^{-6}	5.0000×10^{-8}
0.8	1.0158×10^{-4}	1.3900×10^{-6}	2.9200×10^{-6}	3.4000×10^{-7}	4.0000×10^{-8}
0.9	8.4300×10^{-6}	1.2000×10^{-7}	2.5000×10^{-7}	3.0000×10^{-8}	4.0000×10^{-8}
1.0	7.0000×10^{-7}	1.0000×10^{-8}	3.0000×10^{-8}	0.0000	4.0000×10^{-8}

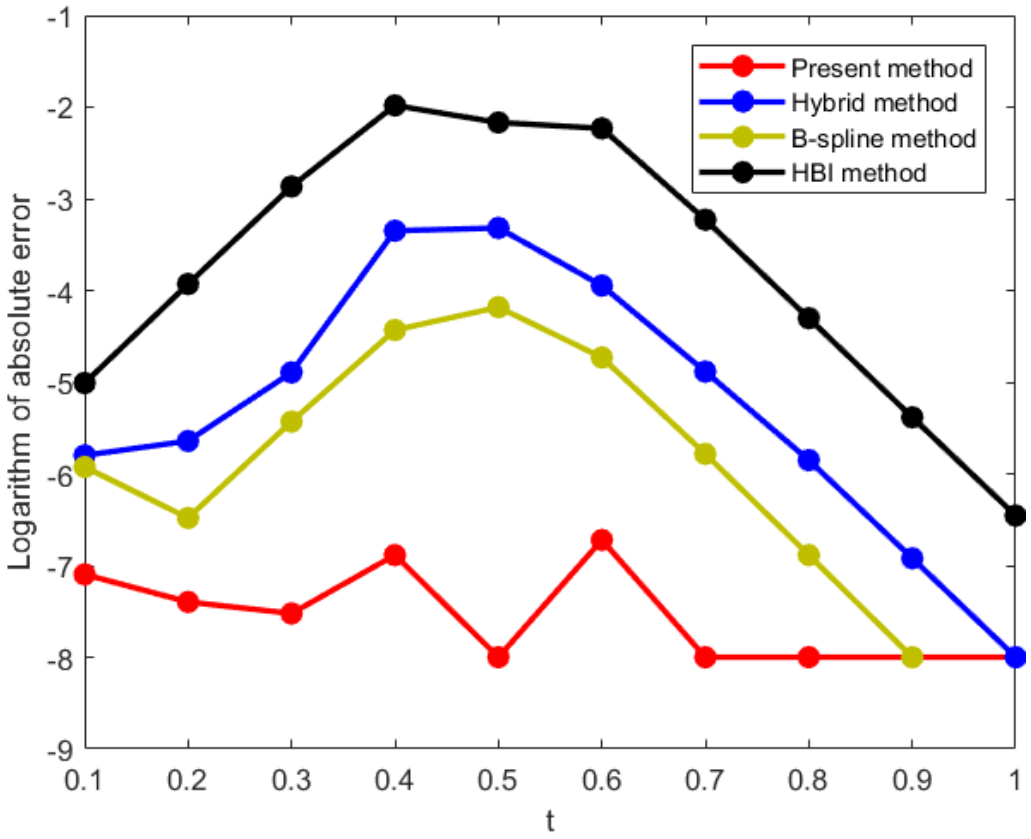

Figure 1. Logarithm of absolute errors of $v(x,t)$ at $t = 0.005$ for Example 1.

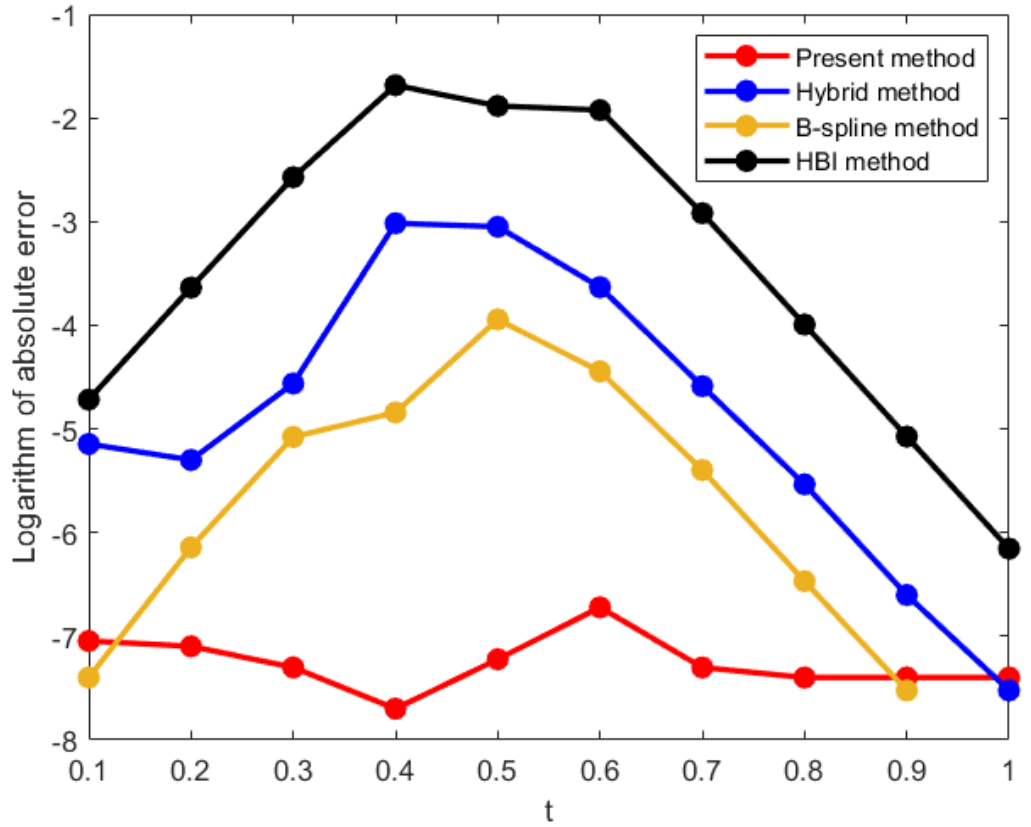

Figure 2. Logarithm of absolute errors of $v(x,t)$ at $t = 0.01$ for Example 1.

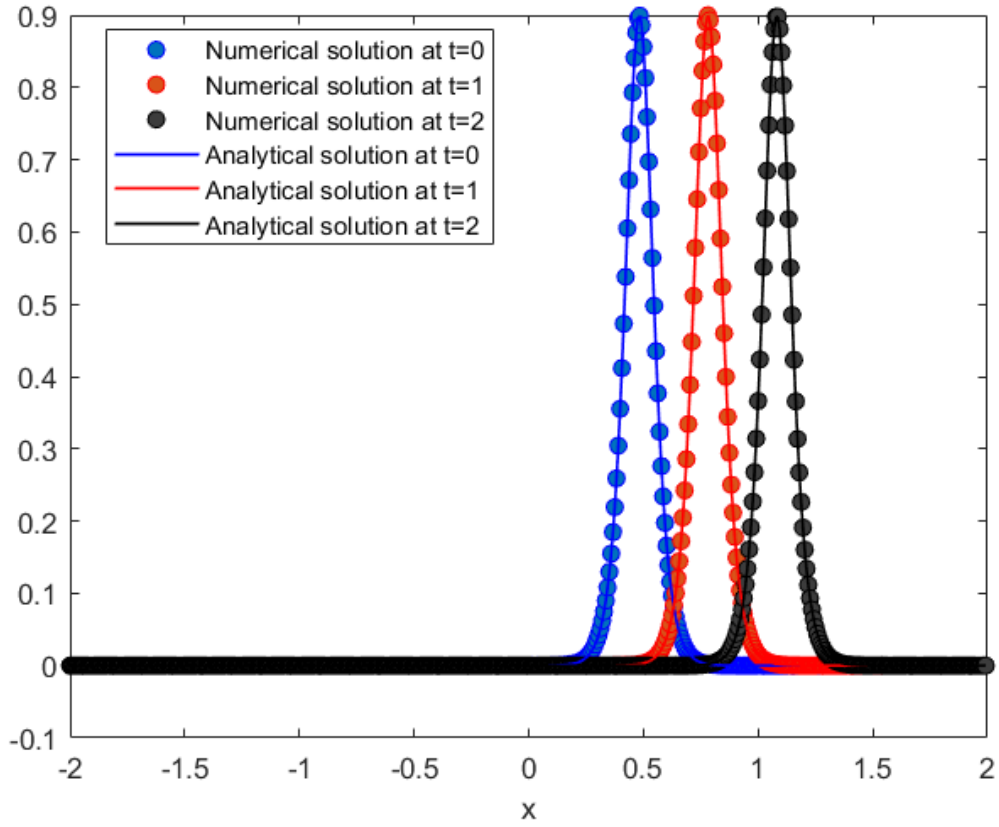

Figure 3. Numerical solutions of $v(x,t)$ obtained by the present method and analytical solutions at $t = 0, 1, 2$ for Example 1.

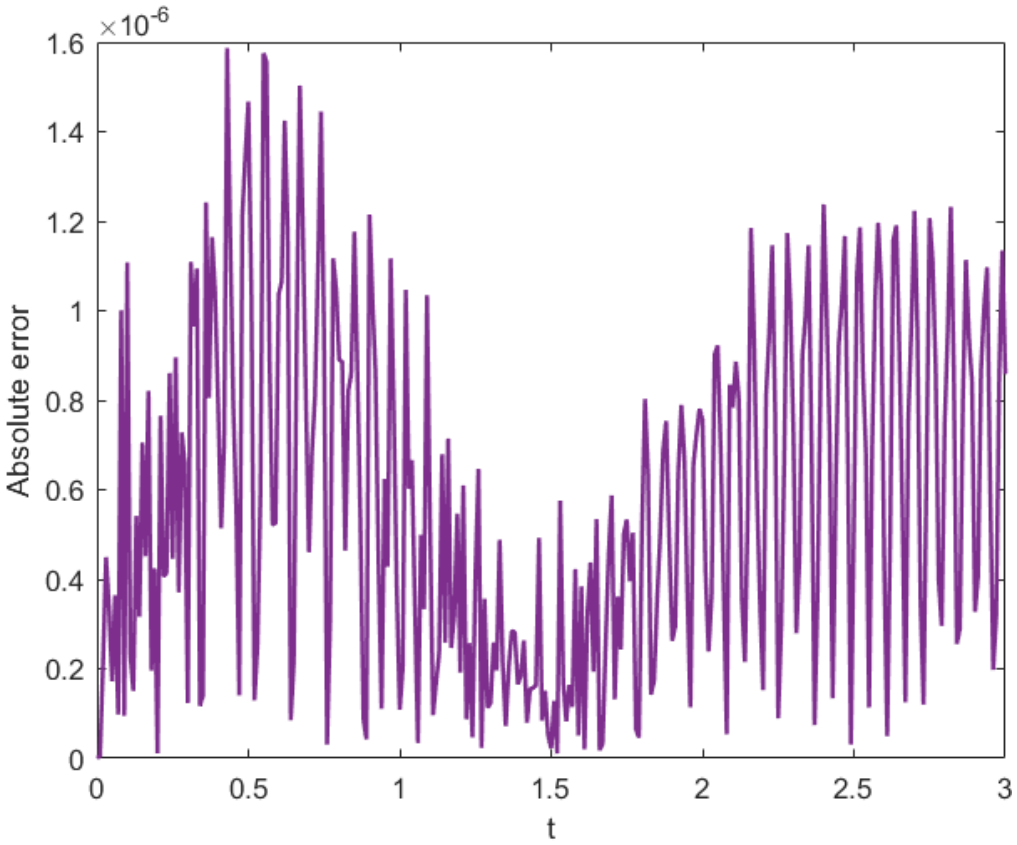

Figure 4. Absolute error of $v(x,t)$ obtained by the present method at $x = 2$ for Example 1.

Table 4. Comparison of L_∞ of $v(x,t)$ at $\alpha_1 = 1, \alpha_2 = 1, k_1 = 0.5, k_2 = 1$ for Example 1.

t	$\beta_1 = 0.9999$	$\beta_1 = 0.99999$	$\beta_1 = 0.999999$	$\beta_1 = 0.9999999$	$\beta_1 = 1$
1.0	3.7351×10^{-3}	3.7415×10^{-4}	3.6993×10^{-5}	4.0937×10^{-6}	2.0209×10^{-6}
1.5	6.9479×10^{-3}	6.9721×10^{-4}	7.0101×10^{-5}	7.4340×10^{-6}	1.2061×10^{-6}
2.0	1.1371×10^{-2}	1.1409×10^{-3}	1.1363×10^{-4}	1.1542×10^{-5}	8.8914×10^{-7}
2.5	1.6674×10^{-2}	1.6785×10^{-3}	1.6737×10^{-4}	1.6364×10^{-5}	8.7256×10^{-7}
3.0	2.2625×10^{-2}	2.2826×10^{-3}	2.2962×10^{-4}	2.4065×10^{-5}	1.1692×10^{-6}

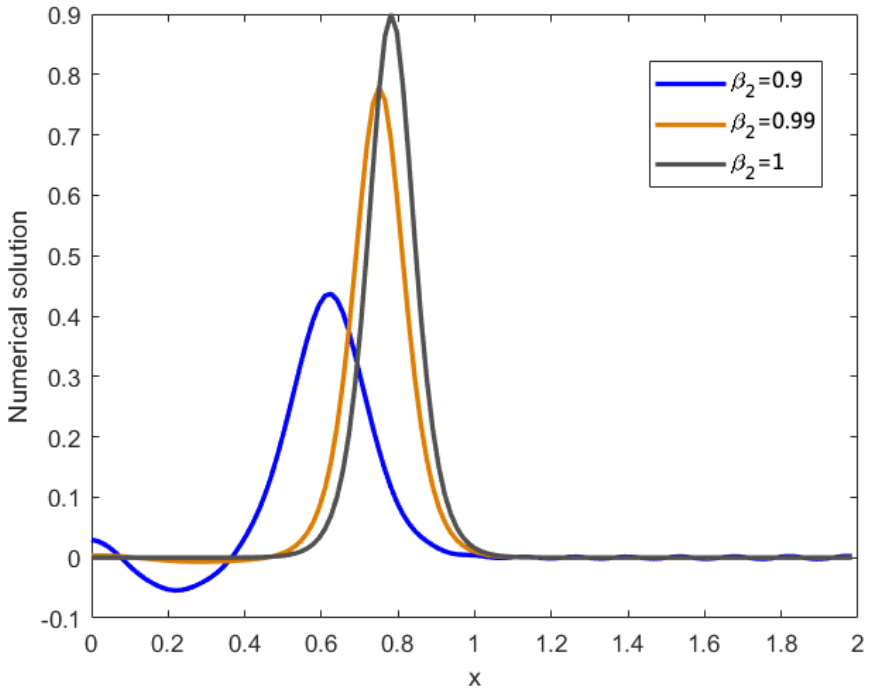

Figure 5. Numerical solutions of vs. at $t = 1$, $\beta_2 = 0.9, 0.99, 1$ for Example 1.

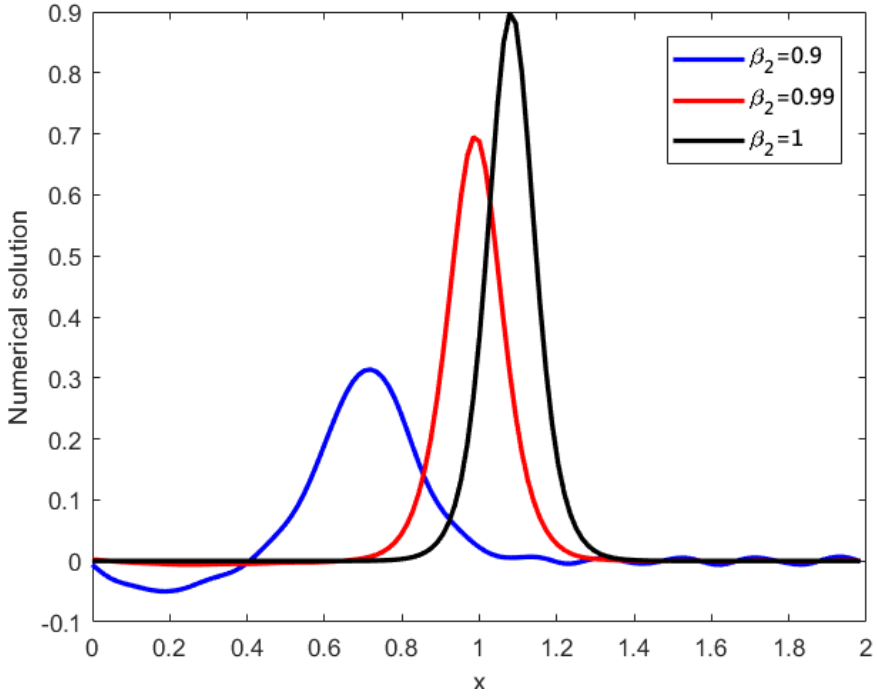

Figure 6. Numerical solutions of vs. at $t = 2$, $\beta_2 = 0.9, 0.99, 1$ for Example 1.

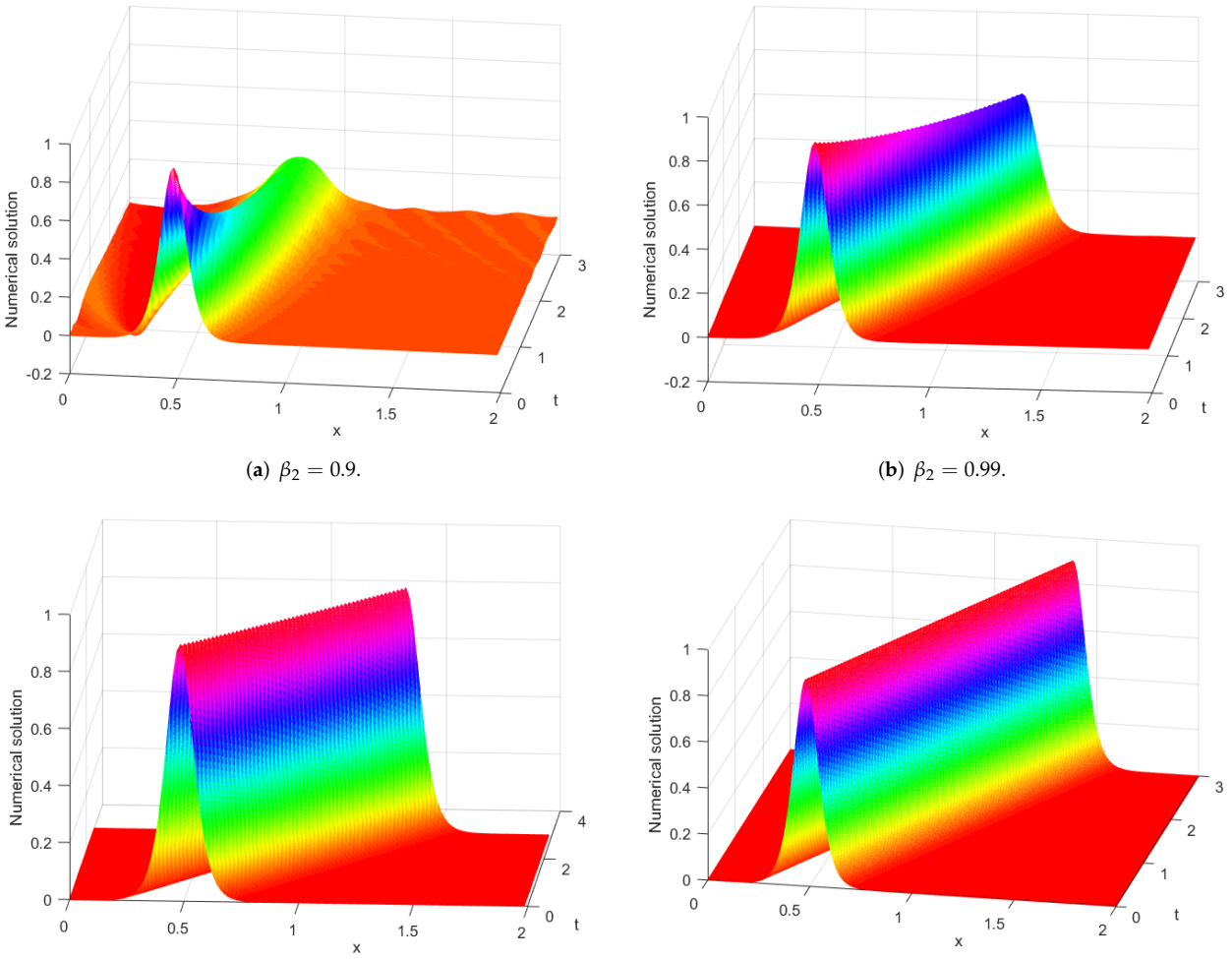

(**a**) $\beta_2 = 0.9$. (**b**) $\beta_2 = 0.99$.

(**c**) $\beta_2 = 0.999$. (**d**) $\beta_2 = 1$.

Figure 7. Numerical solutions of vs. at different β_2 for Example 1.

From Example 1, we know that our numerical method has higher accuracy than other methods for the one-soliton solution. Next, we will study the generalized vc KdV-mKdV equation and the influence of β_1, β_2 on the numerical solution of this equation.

Example 2. *Let* $\varepsilon(t) = -6$, $\alpha_1(t) = 0.06$, $\beta_1 = 2$, $\beta_2 = 1$, $\alpha_2(t) = 0.01$, $\alpha_3(t) = -15\cos\frac{\pi t}{2}$ *in Equation* (1) *and* $\tau = 0.01$, $N = 512$. *The initial value is as follows,*

$$v(x,0) = -\frac{202}{\Psi}\exp(x + \frac{1}{100}). \tag{27}$$

Wang [31] obtained one periodic depression soliton solution of the generalized vcKdV-mKdV equation,

$$v^*(x,t) = -\frac{202}{\Psi}\exp(\frac{t}{100} + \frac{30}{\pi}\sin\frac{\pi t}{2} + x + \frac{1}{100}), \quad -20 \le x \le 20, \tag{28}$$

with

$$\Psi = 20200\exp(\frac{t}{100} + \frac{30}{\pi}\sin\frac{\pi t}{2} + x + \frac{1}{100}) + 10001\exp(\frac{60}{\pi}\sin\frac{\pi t}{2} + 2x + \frac{1}{50}) + 10201\exp(\frac{t}{50}). \tag{29}$$

Table 5 shows L_∞ and GRE at different times. Table 6 shows numerical results. Figures 8–10 represent numerical solution. Absolute errors at $t = 3.4, 3.5, 3.6$ are shown in Figures 11–14 present absolute errors at $x = -10, -5, 10$. From Figure 15 which shows the numerical solutions at different β_1 and β_2, we can find that the change of β_1 and β_2 has minimal effect on the shape of periodic depression soliton.

Table 5. Error norms L_∞ and GRE at different times for Example 2.

	L_∞		GRE	
	Present Method	**Ref. [32]**	**Present Method**	**Ref. [32]**
$t = 1.0$	8.2189×10^{-7}	5.1096×10^{-6}	2.9499×10^{-4}	7.4281×10^{-4}
$t = 2.0$	9.0010×10^{-7}	7.3044×10^{-6}	4.1717×10^{-4}	1.2207×10^{-3}
$t = 3.0$	1.0152×10^{-6}	1.1358×10^{-5}	5.2455×10^{-4}	1.8416×10^{-3}
$t = 4.0$	9.2295×10^{-7}	1.4313×10^{-5}	6.8842×10^{-4}	2.4443×10^{-3}

Table 6. Numerical results of $v(x, t)$ obtained by the present method at $t = 1$ for Example 2.

x	**Analytical Solution**	**Numerical Solution**	**Absolute Error**
-13.75	-0.0003	-0.0003	1.9412×10^{-9}
-12.5	-0.0009	-0.0009	6.7763×10^{-9}
-11.25	-0.0026	-0.0026	1.3403×10^{-8}
-10	-0.0047	-0.0047	1.9307×10^{-9}
-8.75	-0.0043	-0.0043	3.8465×10^{-8}
-7.5	-0.0020	-0.0020	1.6845×10^{-8}
-6.25	-0.0007	-0.0007	2.2970×10^{-8}
-5	-0.0002	-0.0002	3.6866×10^{-9}

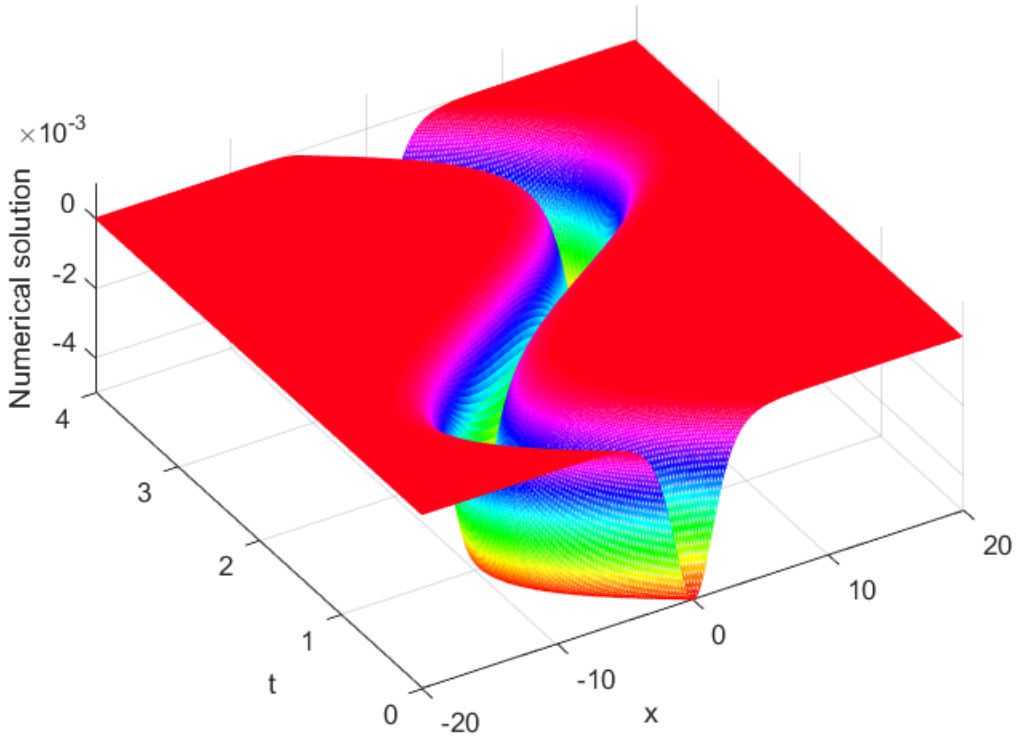

Figure 8. Numerical solution of $v(x, t)$ obtained by the present method for Example 2.

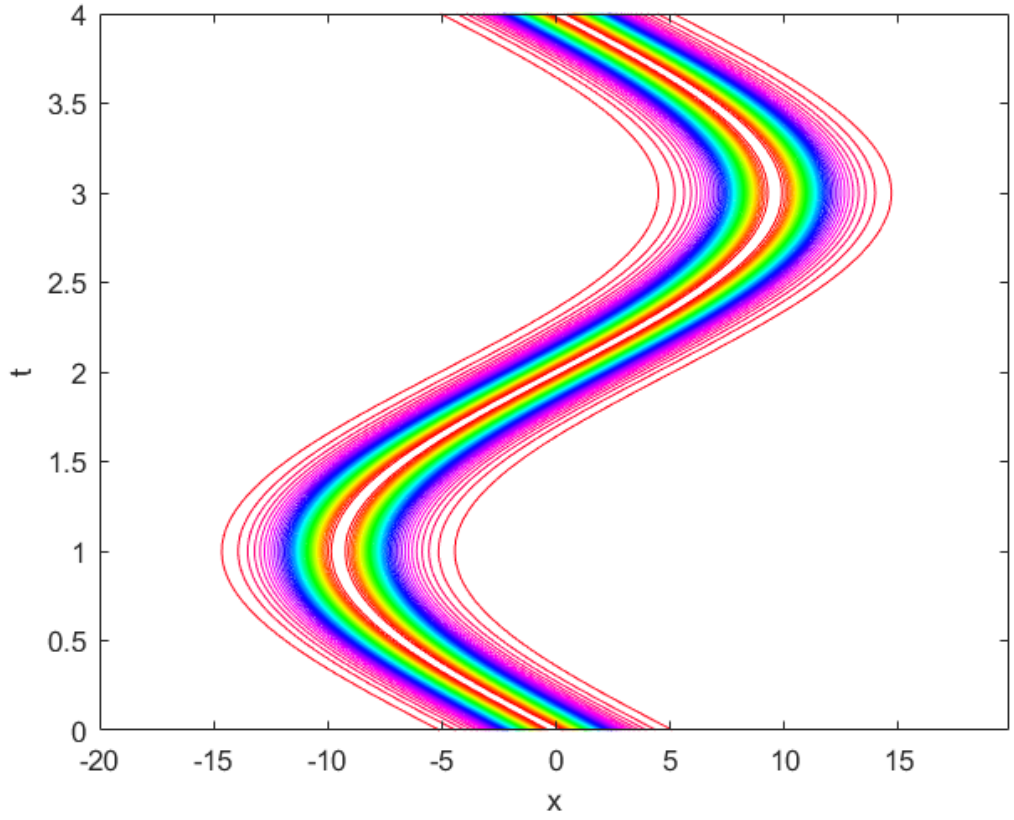

Figure 9. 2D contour plot of $v(x,t)$ obtained by the present method for Example 2.

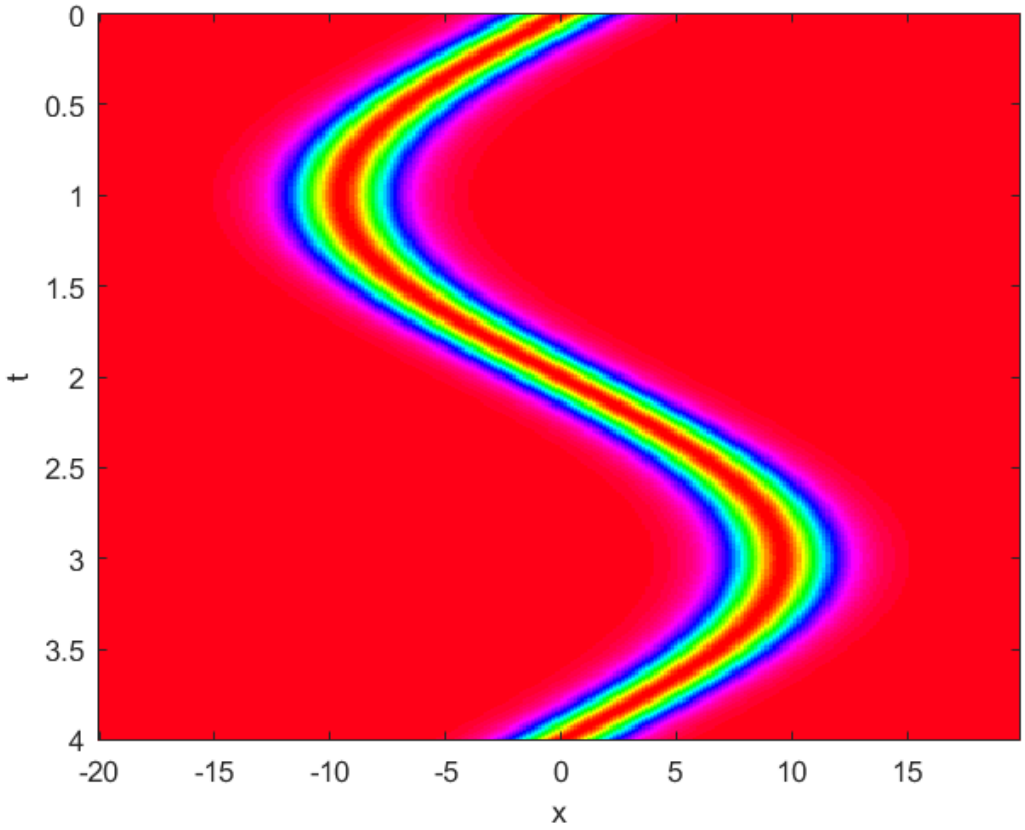

Figure 10. 2D density plot of $v(x,t)$ obtained by the present method for Example 2.

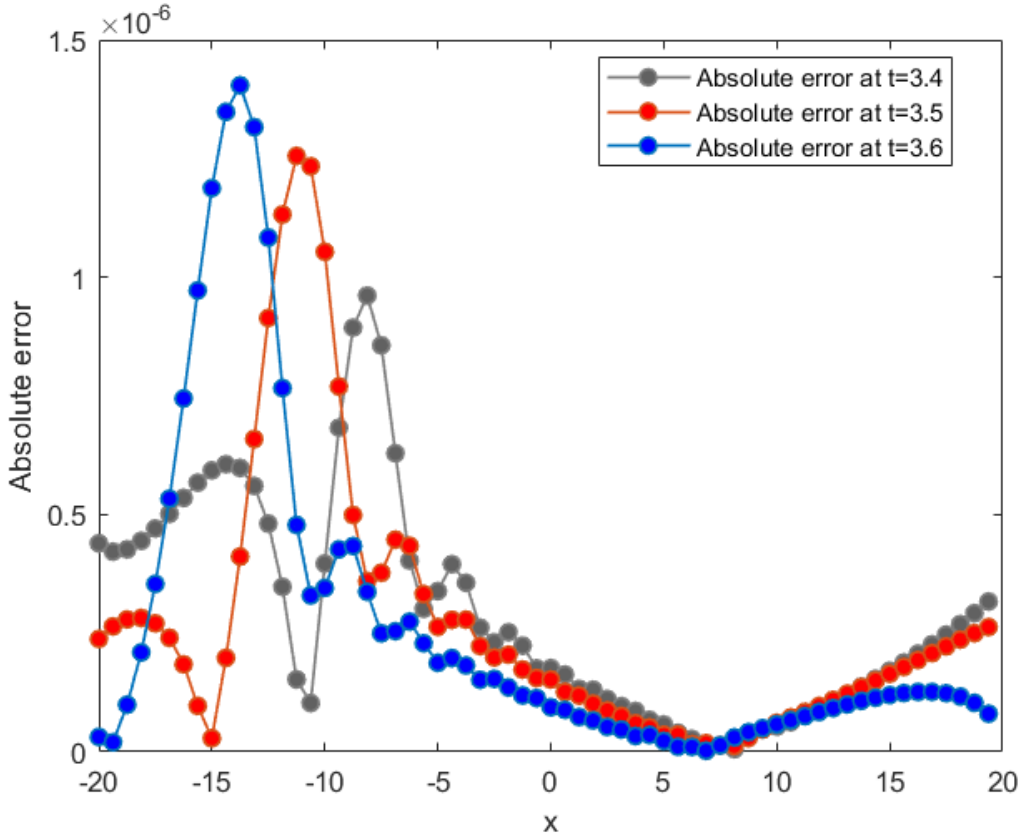

Figure 11. Absolute errors of $v(x,t)$ obtained by the present method at $t = 3.4, 3.5, 3.6$ for Example 2.

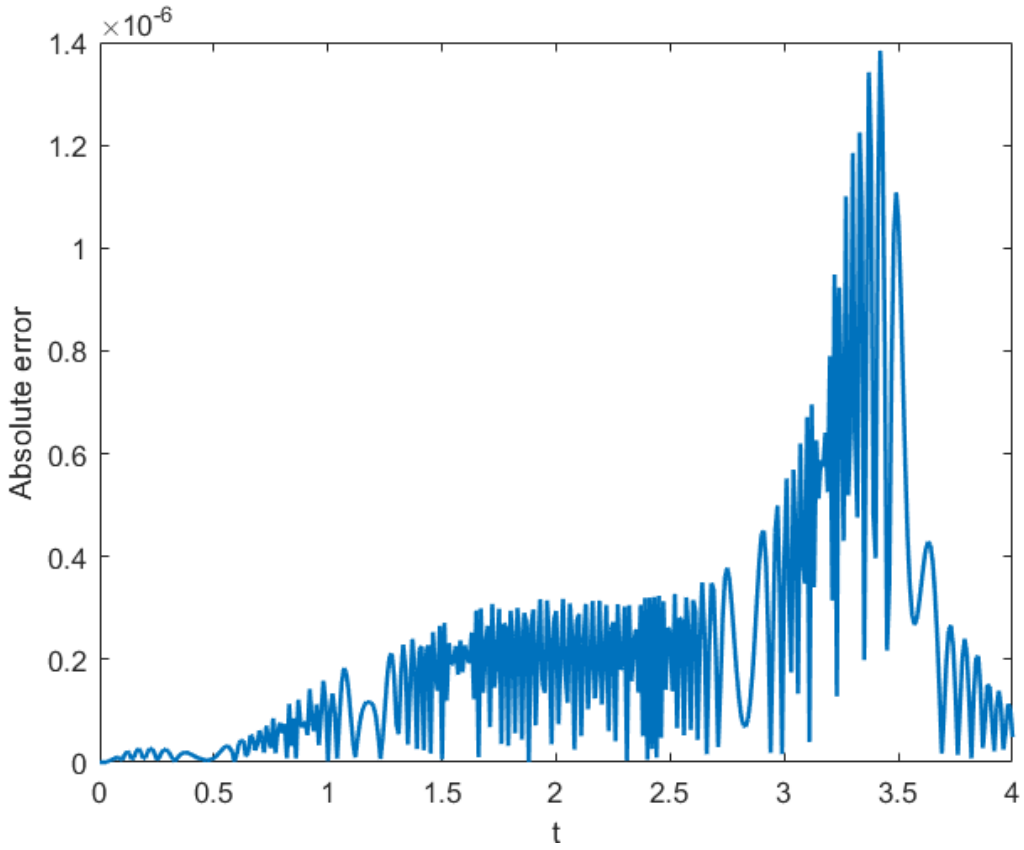

Figure 12. Absolute error of $v(x,t)$ obtained by the present method at $x = -10$ for Example 2.

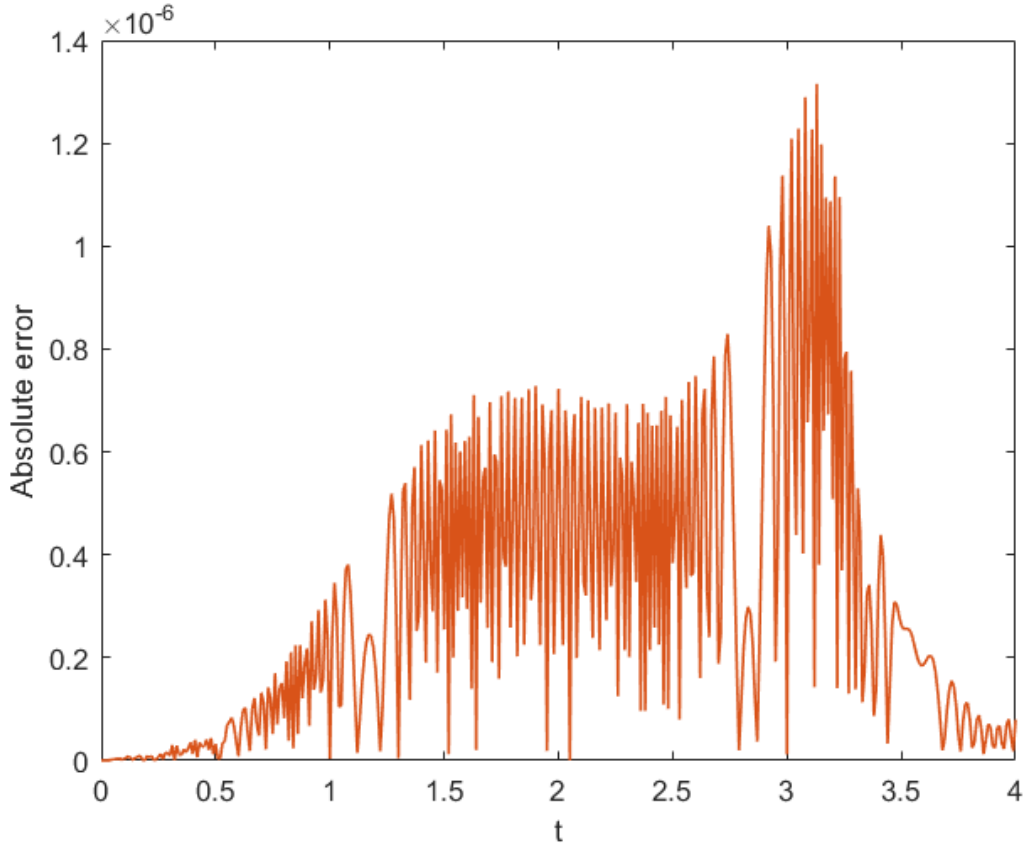

Figure 13. Absolute error of $v(x,t)$ obtained by the present method at $x = -5$ for Example 2.

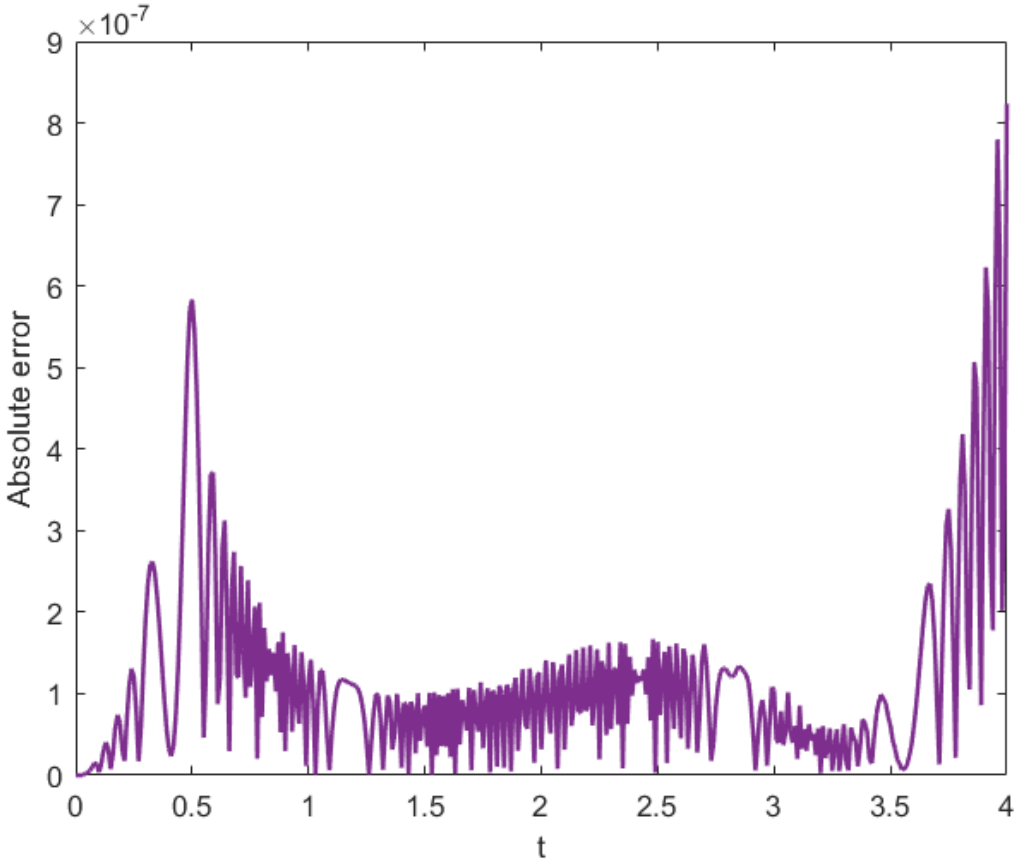

Figure 14. Absolute error of $v(x,t)$ obtained by the present method at $x = 10$ for Example 2.

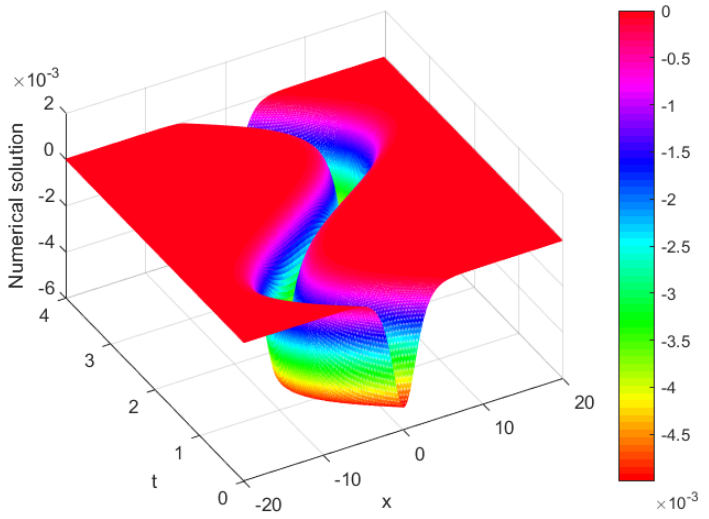

(**a**) $\beta_1 = 0.7, \beta_2 = 0.5$.

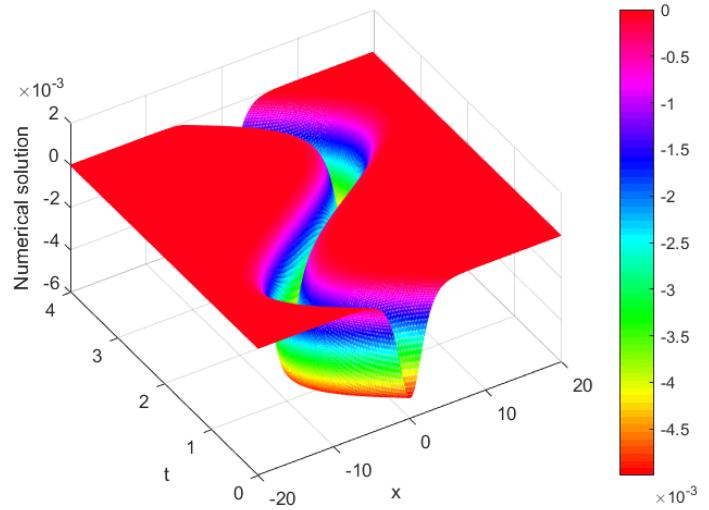

(**b**) $\beta_1 = 1.0, \beta_2 = 0.5$.

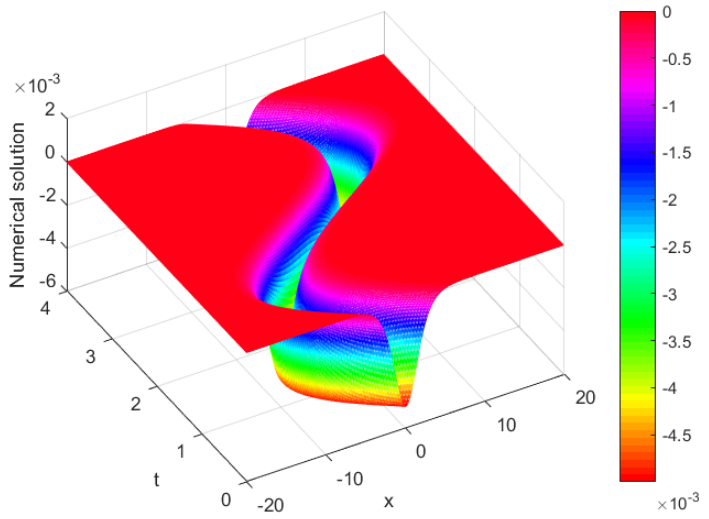

(**c**) $\beta_1 = 1.0, \beta_2 = 0.6$.

Figure 15. Numerical solutions of vs. at different β_1, β_2 for Example 2.

From Example 2, we find that our numerical method has higher accuracy and low computational complexity than other methods for one periodic depression soliton solution of the generalized vc KdV-mKdV equation. Next, we will investigate the breather-type solution of the mKdV equation.

Example 3. *Let* $\alpha_3 = \alpha_4 = \varepsilon = 0$ *and* $\beta_1 = 1$ *in Equation* (1).

Case I *The initial value is as follows,*

$$v(x,-4) = \pm 2\sqrt{\frac{6\alpha_2}{\alpha_1}}\frac{\partial}{\partial x}\arctan\left(\frac{k_2}{k_1}\frac{\sin(k_1\alpha_2^{-\frac{1}{3}}x - \omega_1(-4))}{\cosh(\omega_2(-4) - k_2\alpha_2^{-\frac{1}{3}}x)}\right), \quad -20 \le x \le 20, \tag{30}$$

with

$$\omega_1 = 3k_2^2k_1 - k_1^3, \quad \omega_2 = k_2^3 - 3k_1^2k_2, \tag{31}$$

where k_1, k_2 *are constant parameters.*

The breather-type solution is as follows [33]:

$$v^*(x,t) = \pm 2\sqrt{\frac{6\alpha_2}{\alpha_1}}\frac{\partial}{\partial x}\arctan\left(\frac{k_2}{k_1}\frac{\sin(k_1\alpha_2^{-\frac{1}{3}}x - \omega_1 t)}{\cosh(\omega_2 t - k_2\alpha_2^{-\frac{1}{3}}x)}\right). \tag{32}$$

In this simulation, we set $\alpha_1 = 1$, $\alpha_2 = 1$, $k_1 = 0.5$, $k_2 = 1$, $\tau = 0.01$ and $N = 512$. Table 7 gives the numerical results and Figures 16–18 show the numerical solution. Figure 19 shows the absolute errors at $t = 1$. The absolute error at $x = 5$ is plotted in Figure 20. Table 8 gives L_2, L_∞ and GRE at different times. Then, we shall investigate the space fractional modified KdV equation. We take (32) as the analytical solution for the space fractional modified KdV equation. Figures 21 and 22 show the numerical solutions at $\beta_1 = 0.6, 0.99, 1$ and $t = 0, 1$. Table 9 gives L_∞ at different β_1. Figure 23 shows numerical solutions at different β_1.

Table 7. Numerical results of $v(x,t)$ at $t = 1$,$\alpha_1 = 1$, $\alpha_2 = 1$, $k_1 = 0.5$, $k_2 = 1$ for Case I.

x	Analytical Solution	Numerical Solution	Absolute Error
−10.0	0.0003	0.0003	4.7709×10^{-9}
−7.5	0.0094	0.0094	1.7568×10^{-8}
−5.0	0.0306	0.0306	1.7562×10^{-8}
−2.5	−1.1357	−1.1357	4.1767×10^{-9}
0	−0.2941	−0.2941	2.4809×10^{-8}
2.5	1.2591	1.2591	6.0335×10^{-8}
5.0	−0.1163	−0.1163	7.8856×10^{-8}
7.5	−0.0147	−0.0147	5.0883×10^{-8}

Table 8. Error norms, L_2, L_∞ and GRE at $\alpha_1 = 1$, $\alpha_2 = 1$, $k_1 = 0.5$, $k_2 = 1$ for Example 3.

	$t = 0$	$t = 1.0$	$t = 2.0$	$t = 3.0$	$t = 4.0$
L_2	4.3364×10^{-7}	4.1878×10^{-8}	3.6983×10^{-7}	7.3778×10^{-7}	7.7441×10^{-7}
L_∞	5.0048×10^{-7}	9.0930×10^{-8}	4.5768×10^{-7}	8.1363×10^{-7}	8.4852×10^{-7}
GRE	1.5727×10^{-6}	1.1964×10^{-7}	1.3157×10^{-6}	2.6396×10^{-6}	2.7113×10^{-6}

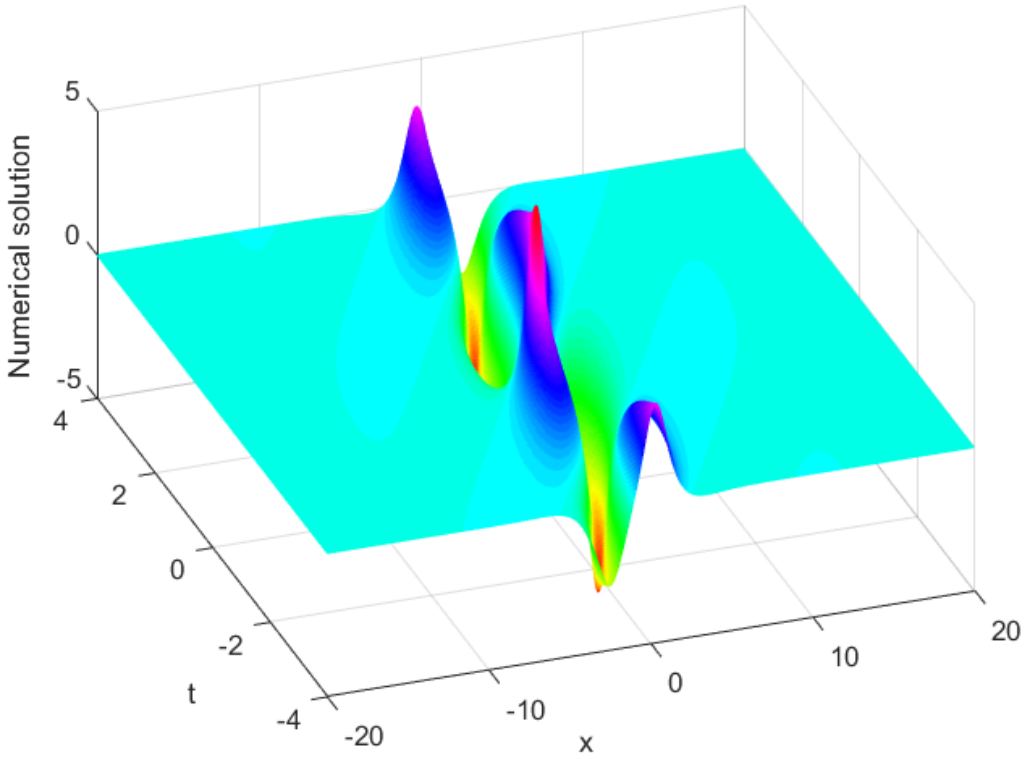

Figure 16. Numerical solution at $\alpha_1 = 1$, $\alpha_2 = 1$, $k_1 = 0.5$, $k_2 = 1$ for Example 3.

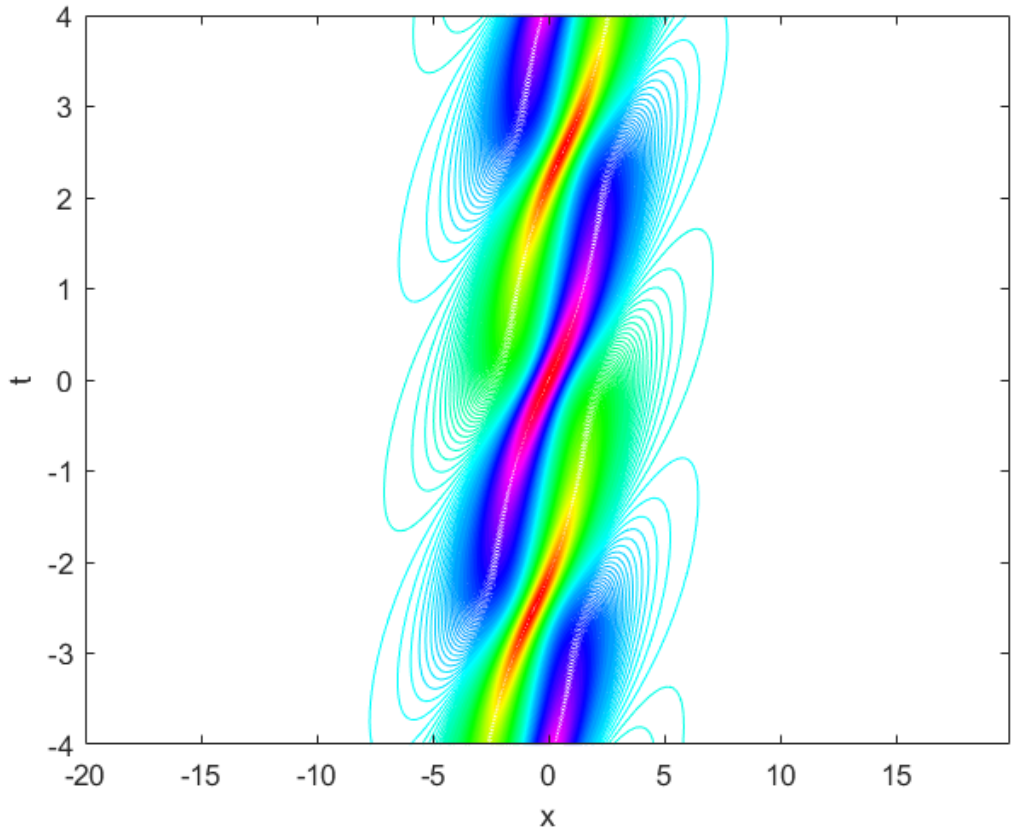

Figure 17. 2D contour plot at $\alpha_1 = 1$, $\alpha_2 = 1$, $k_1 = 0.5$, $k_2 = 1$ for Example 3.

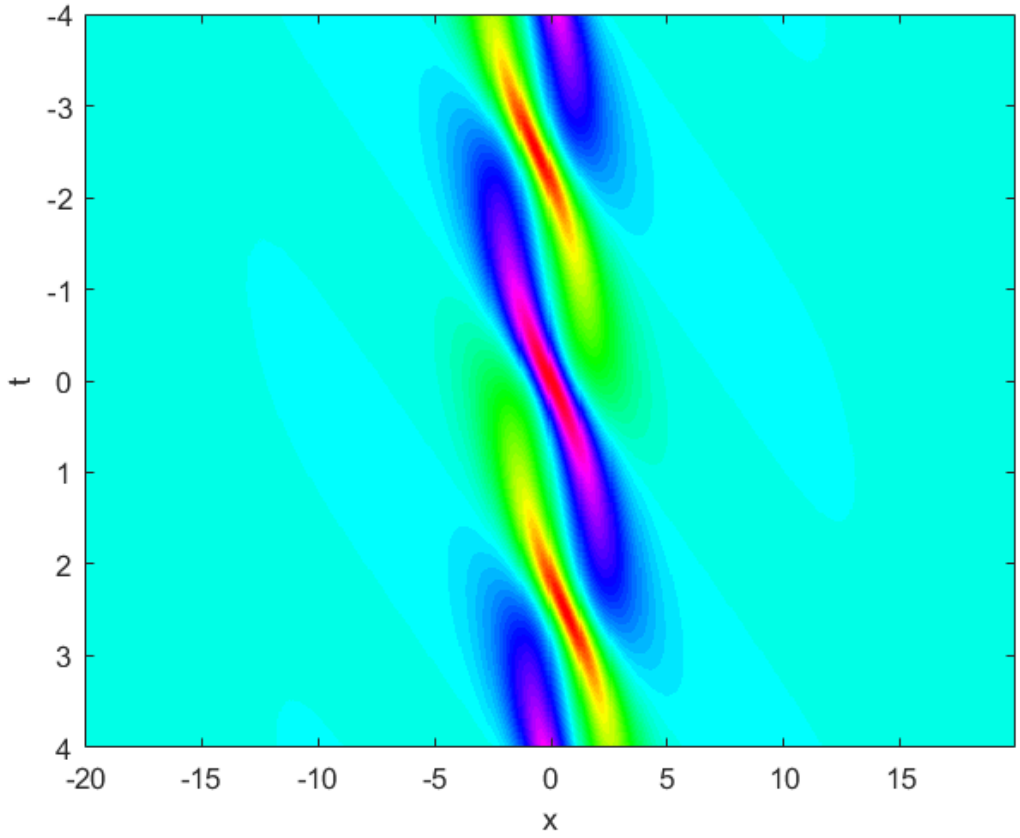

Figure 18. 2D density plot at $\alpha_1 = 1$, $\alpha_2 = 1$, $k_1 = 0.5$, $k_2 = 1$ for Example 3.

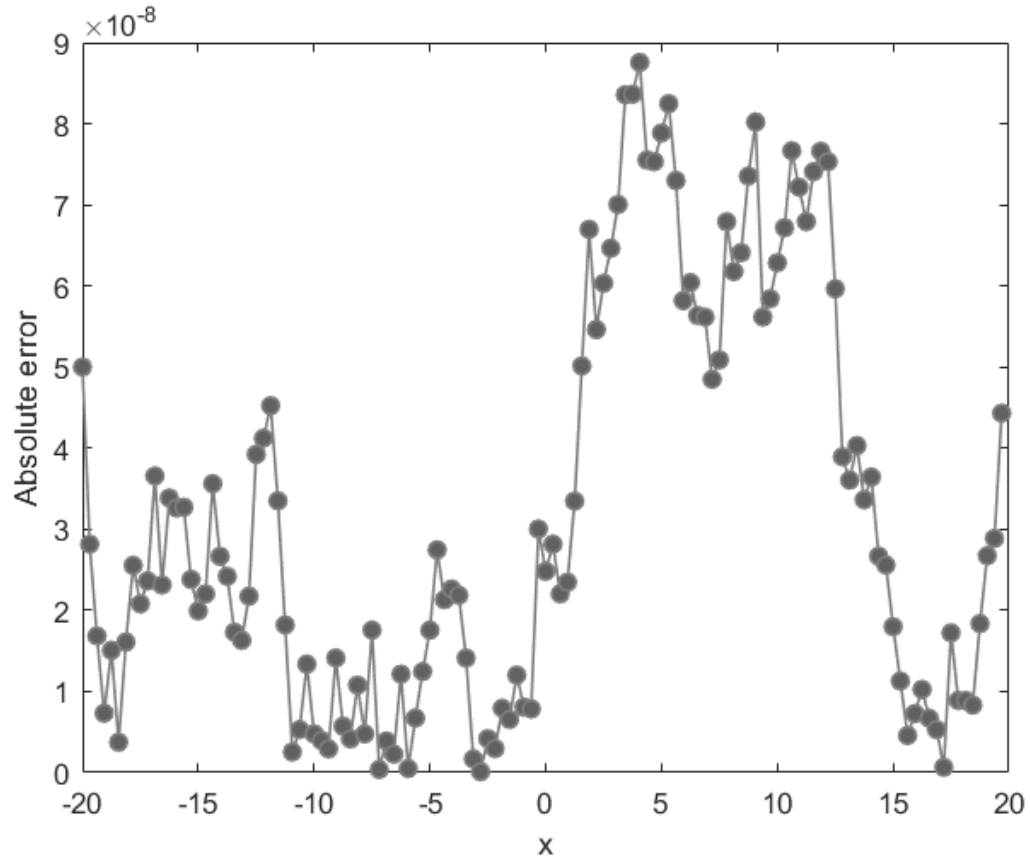

Figure 19. Absolute error at $\alpha_1 = 1$, $\alpha_2 = 1$, $k_1 = 0.5$, $k_2 = 1$, $t = 1$ for Example 3.

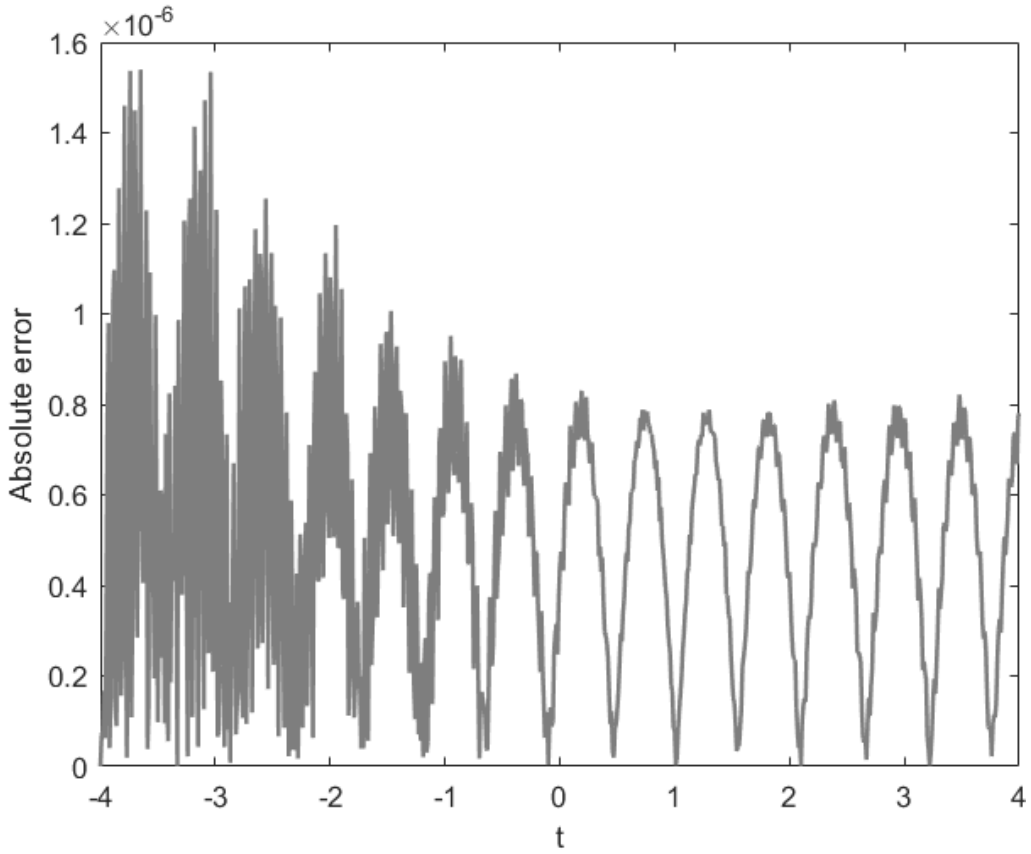

Figure 20. Absolute error at $\alpha_1 = 1, \alpha_2 = 1, k_1 = 0.5, k_2 = 1, x = 5$ for Example 3.

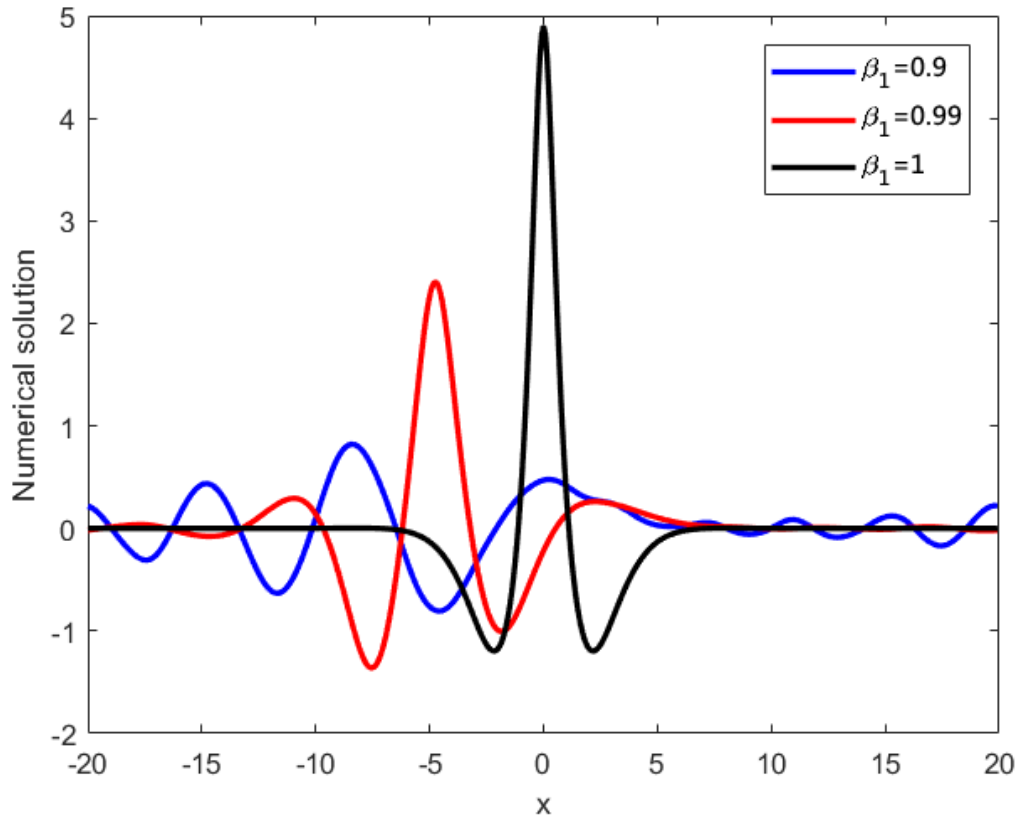

Figure 21. Numerical solutions of vs. at $t = 0, \beta_1 = 0.9, 0.99, 1, \alpha_1 = 1, \alpha_2 = 1, k_1 = 0.5, k_2 = 1$ for Example 3.

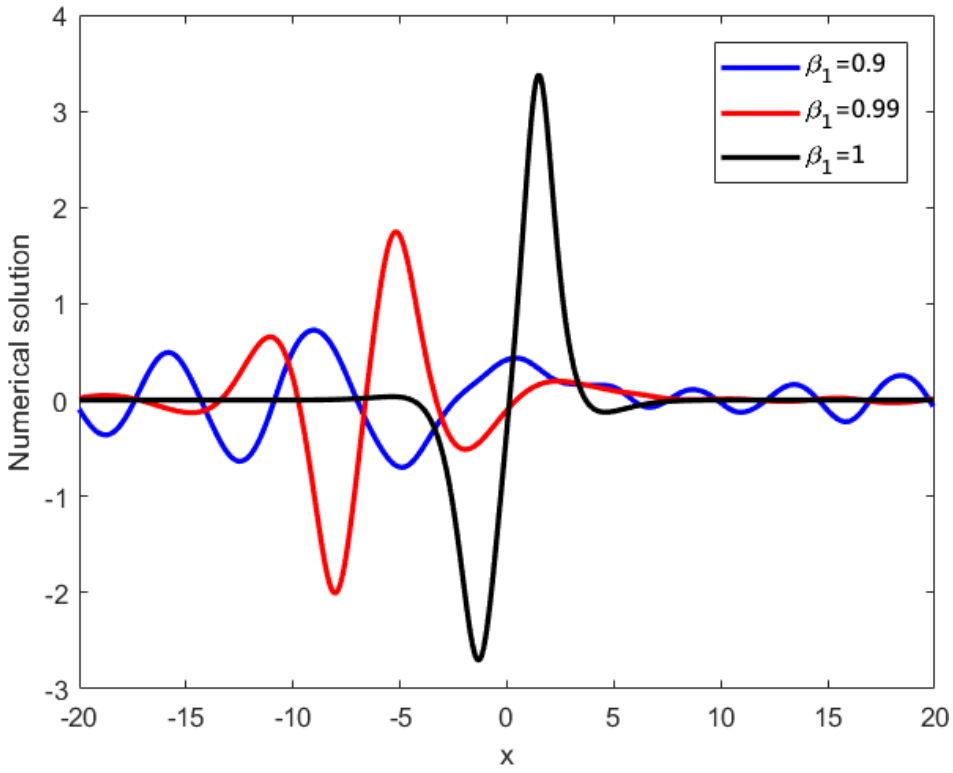

Figure 22. Numerical solutions of vs. at $t = 1$, $\beta_1 = 0.9, 0.99, 1$, $\alpha_1 = 1$, $\alpha_2 = 1$, $k_1 = 1$, $k_2 = -2$ for Example 3.

Table 9. Comparison of L_∞ of $v(x,t)$ at $\alpha_1 = 1$, $\alpha_2 = 1$, $k_1 = 0.5$, $k_2 = 1$ for Example 3.

t	$\beta_1 = 0.999999$	$\beta_1 = 0.9999999$	$\beta_1 = 0.99999999$	$\beta_1 = 0.999999999$	$\beta_1 = 1$
-2	1.7658×10^{-3}	1.7716×10^{-4}	1.8260×10^{-5}	2.3703×10^{-6}	1.2617×10^{-6}
-1	1.8815×10^{-3}	1.8875×10^{-4}	1.9565×10^{-5}	2.6702×10^{-6}	9.2254×10^{-7}
0	5.4293×10^{-3}	5.4241×10^{-4}	5.3860×10^{-5}	5.7137×10^{-6}	5.0048×10^{-7}
1	6.9070×10^{-3}	6.9092×10^{-4}	6.9067×10^{-5}	6.8848×10^{-6}	9.0930×10^{-8}
2	9.6478×10^{-3}	9.6405×10^{-4}	9.6092×10^{-5}	9.9524×10^{-6}	5.5768×10^{-6}

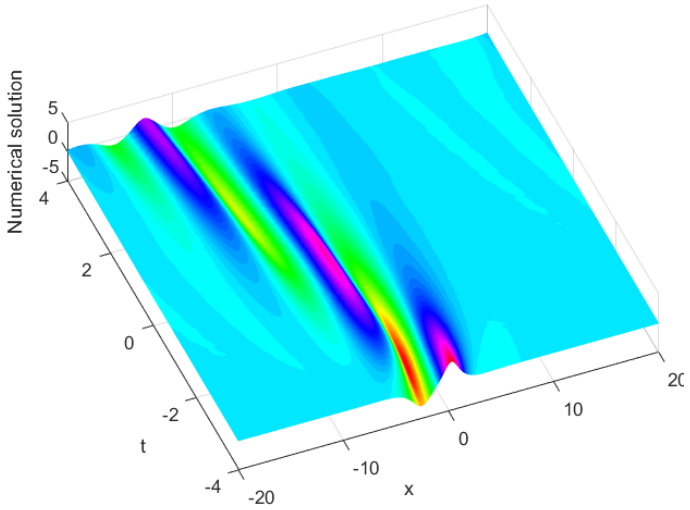

(a) $\beta_1 = 0.99$.

Figure 23. *Cont.*

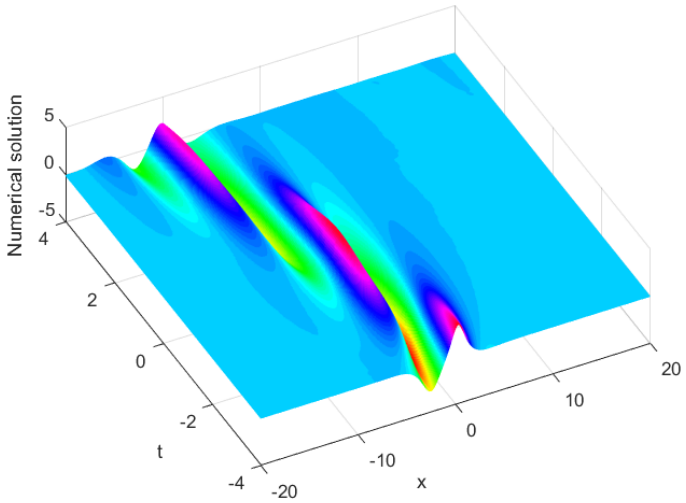

(**b**) $\beta_1 = 0.995$.

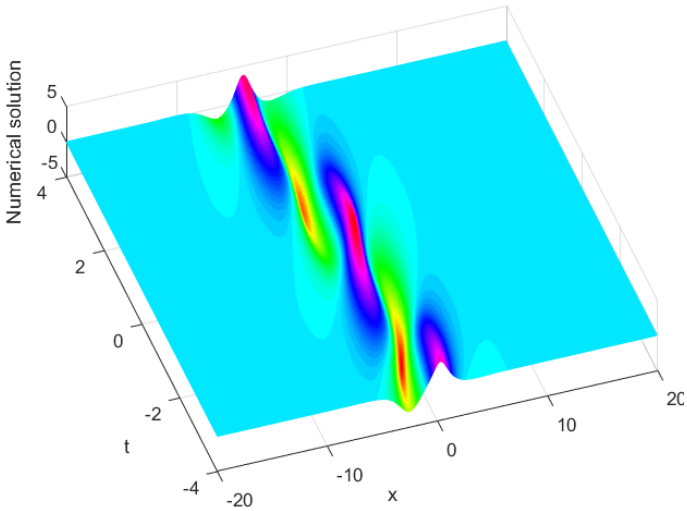

(**c**) $\beta_1 = 0.999$.

Figure 23. Numerical solutions at $\alpha_1 = 1, \alpha_2 = 1, k_1 = 0.5, k_2 = 1$ and different β_1 for Example 3.

Case II The initial value is as follows,

$$v(x,-2) = \pm 2\sqrt{\frac{6\alpha_2}{\alpha_1}}\frac{\partial}{\partial x}\arctan\left(\frac{k_2}{k_1}\frac{\sin(k_1\alpha_2^{-\frac{1}{3}}x - \omega_1(-2))}{\cosh(\omega_2(-2) - k_2\alpha_2^{-\frac{1}{3}}x)}\right), \quad -10 \le x \le 10. \tag{33}$$

In this simulation, we set $\alpha_1 = 1, \alpha_2 = 1, k_1 = 1, k_2 = -2$, $\tau = 0.01$ and $N = 256$. Table 10 shows numerical results. Table 11 gives L_2, L_∞ and GRE at different times. Absolute error at $t = -1$ is plotted in Figure 24. Figures 25 and 26 show absolute errors at $x = -5, 5$. Figure 27 shows numerical solutions at $\beta_1 = 0.9, 0.99, 1$ and $t = 0$. Table 12 presents L_∞ at different β_1. Numerical solution at different β_1 are plotted in Figure 28. Figures 29–31 present the numerical solution.

Table 10. Numerical results of $v(x,t)$ at $\alpha_1 = 1$, $\alpha_2 = 1$, $k_1 = 1$, $k_2 = -2$, $t = 0$ for Case II.

x	Analytical Solution	Numerical Solution	Absolute Error
-5.625	-0.0005	-0.0005	9.8195×10^{-7}
-5.0	-0.0020	-0.0020	1.5196×10^{-6}
-3.75	-0.0035	-0.0035	1.0557×10^{-6}
-1.875	1.0078	1.0078	1.2865×10^{-6}
-1.25	2.2706	2.2706	1.9922×10^{-6}
0	-9.7980	-9.7980	1.6831×10^{-5}
1.25	2.2706	2.2706	2.1611×10^{-6}
1.875	1.0078	1.0078	1.6041×10^{-6}
3.75	-0.0035	-0.0035	1.5075×10^{-6}

Table 11. Error norms, L_2, L_∞ and GRE at $\alpha_1 = 1$, $\alpha_2 = 1$, $k_1 = 1$, $k_2 = -2$ for Example 3.

	$t = -2$	$t = -1$	$t = 0$	$t = 1$	$t = 2$
L_2	4.0774×10^{-16}	8.5229×10^{-7}	2.7727×10^{-6}	1.6213×10^{-6}	1.5889×10^{-6}
L_∞	1.7764×10^{-15}	2.1440×10^{-6}	1.6831×10^{-5}	3.5398×10^{-6}	2.5029×10^{-6}
GRE	5.2480×10^{-16}	1.3009×10^{-6}	3.2589×10^{-6}	2.7586×10^{-6}	2.7296×10^{-6}

Table 12. Comparison of L_∞ of $v(x,t)$ at $\alpha_1 = 1$, $\alpha_2 = 1$, $k_1 = 1$, $k_2 = -2$ for Example 3.

t	$\beta_1 = 0.9999999$	$\beta_1 = 0.99999999$	$\beta_1 = 0.99999999$	$\beta_1 = 0.9999999999$	$\beta_1 = 1$
-1	3.8303×10^{-3}	3.8396×10^{-4}	3.9336×10^{-5}	4.8743×10^{-6}	2.1440×10^{-6}
0	1.6335×10^{-2}	1.6269×10^{-3}	1.7066×10^{-4}	2.7020×10^{-5}	1.6831×10^{-5}
1	3.7859×10^{-2}	3.7830×10^{-3}	3.7557×10^{-4}	3.8415×10^{-5}	3.5398×10^{-6}
2	5.7068×10^{-2}	5.7102×10^{-3}	5.6925×10^{-4}	5.6869×10^{-5}	2.5029×10^{-6}

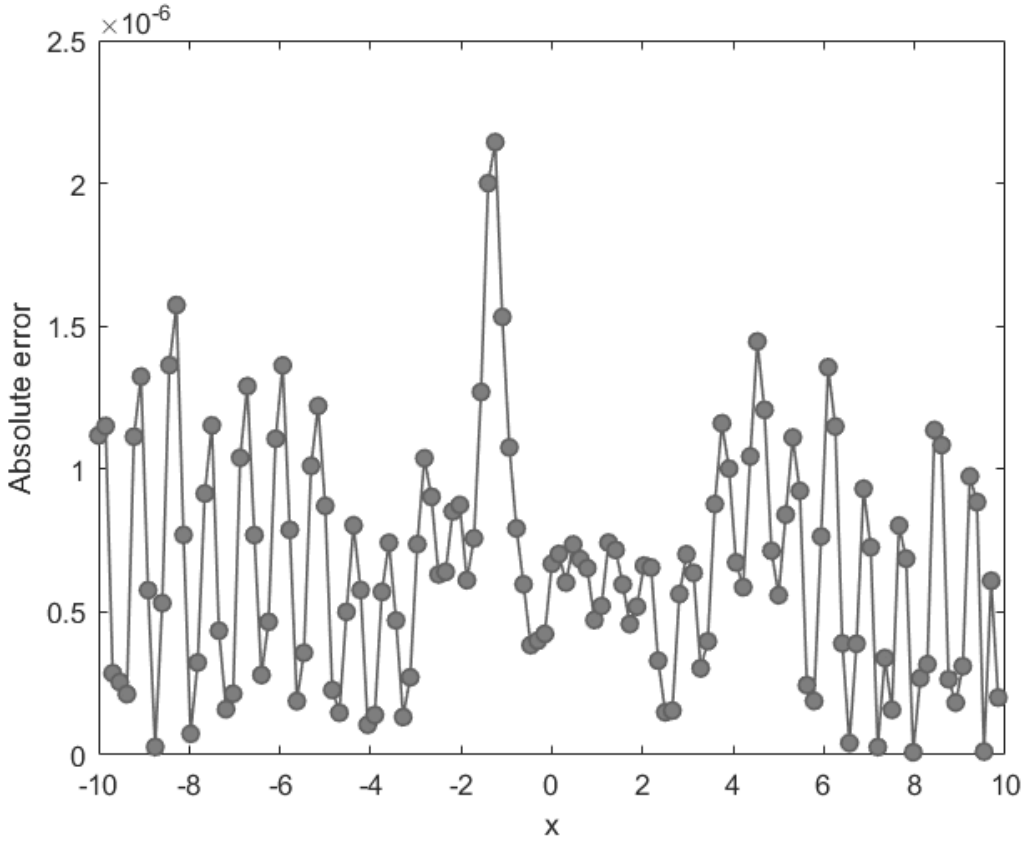

Figure 24. Absolute error at $t = -1$, $\alpha_1 = 1$, $\alpha_2 = 1$, $k_1 = 1$, $k_2 = -2$ for Case II.

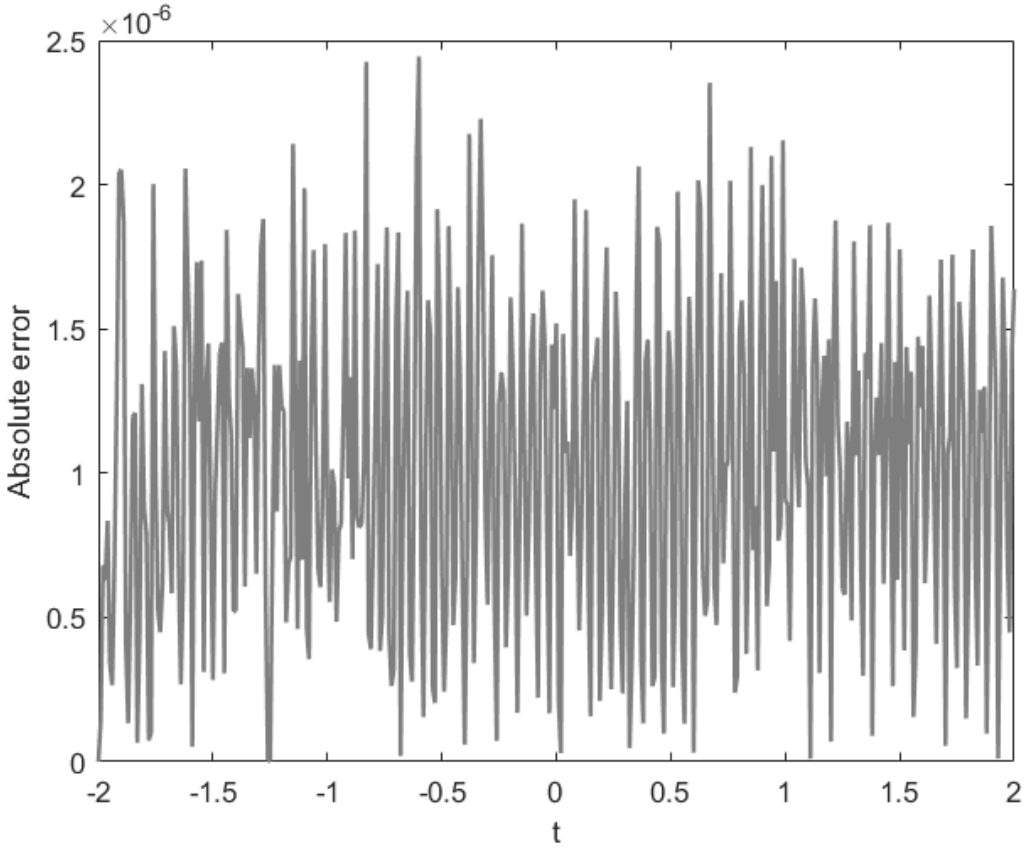

Figure 25. Absolute error at $x = -5$, $\alpha_1 = 1$, $\alpha_2 = 1$, $k_1 = 1$, $k_2 = -2$ for Case II.

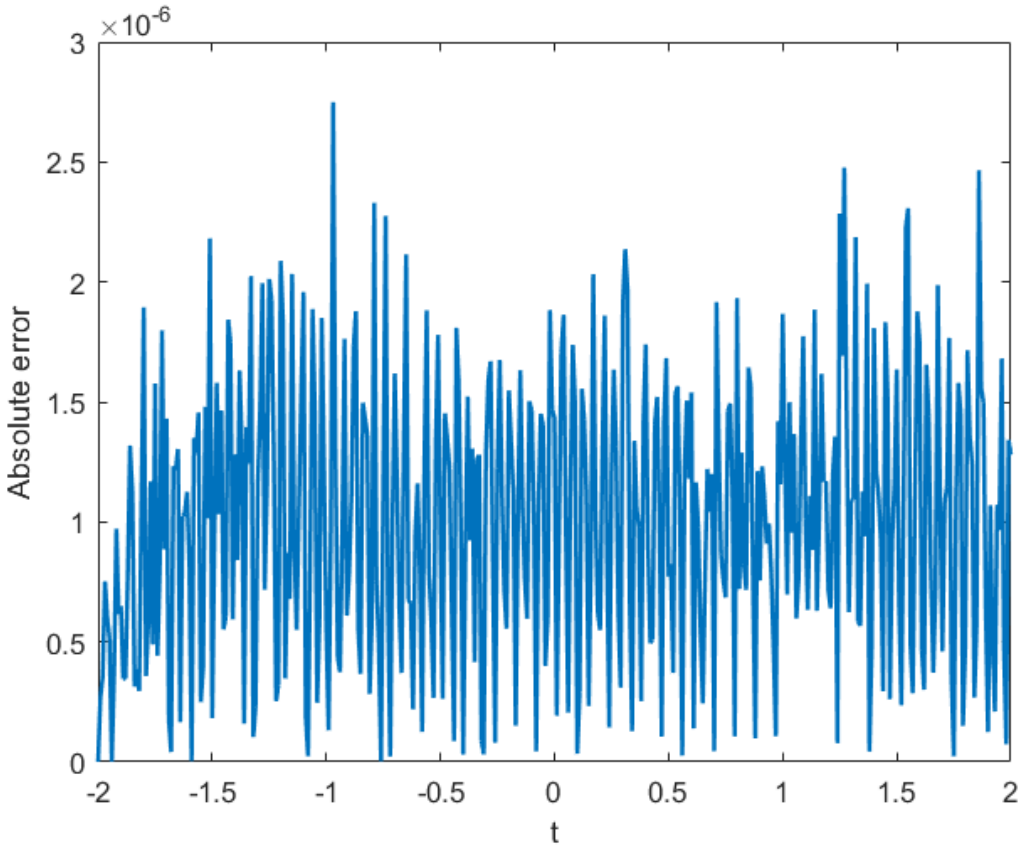

Figure 26. Absolute error at $x = 5$, $\alpha_1 = 1$, $\alpha_2 = 1$, $k_1 = 1$, $k_2 = -2$ for Case II.

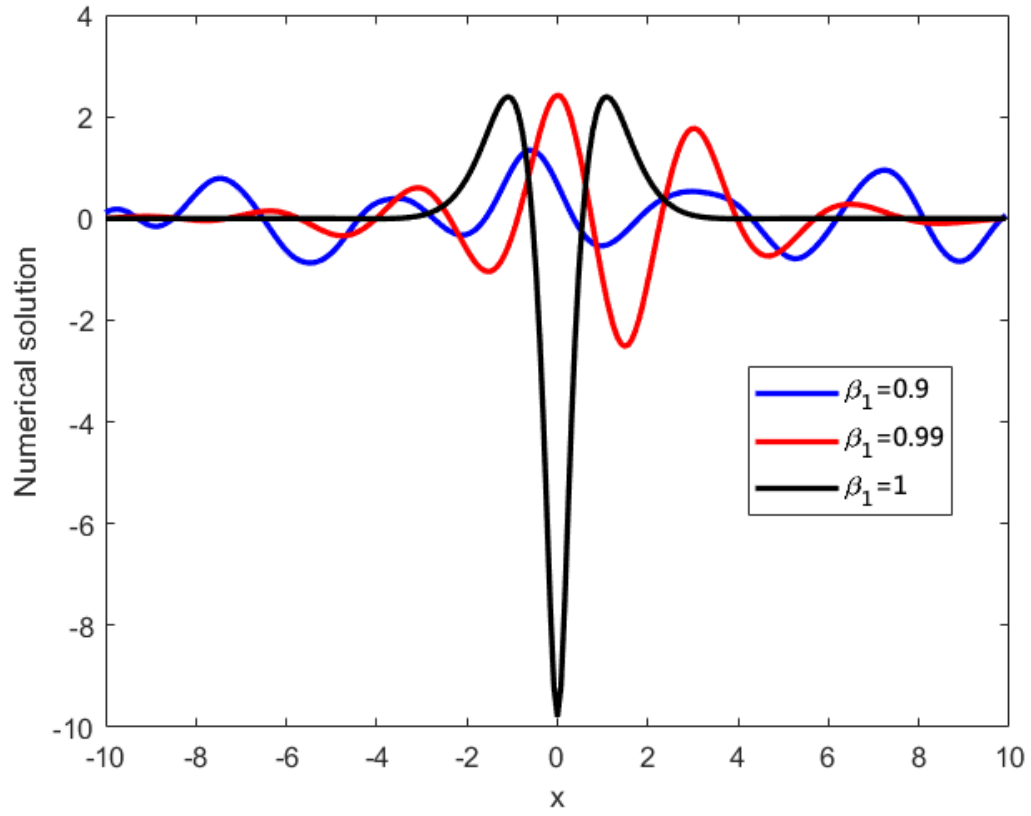

Figure 27. Numerical solutions of vs. at $\beta_1 = 0.9, 0.99, 1$, $t = 0$, $\alpha_1 = 1$, $\alpha_2 = 1$, $k_1 = 1$, $k_2 = -2$ for Case II.

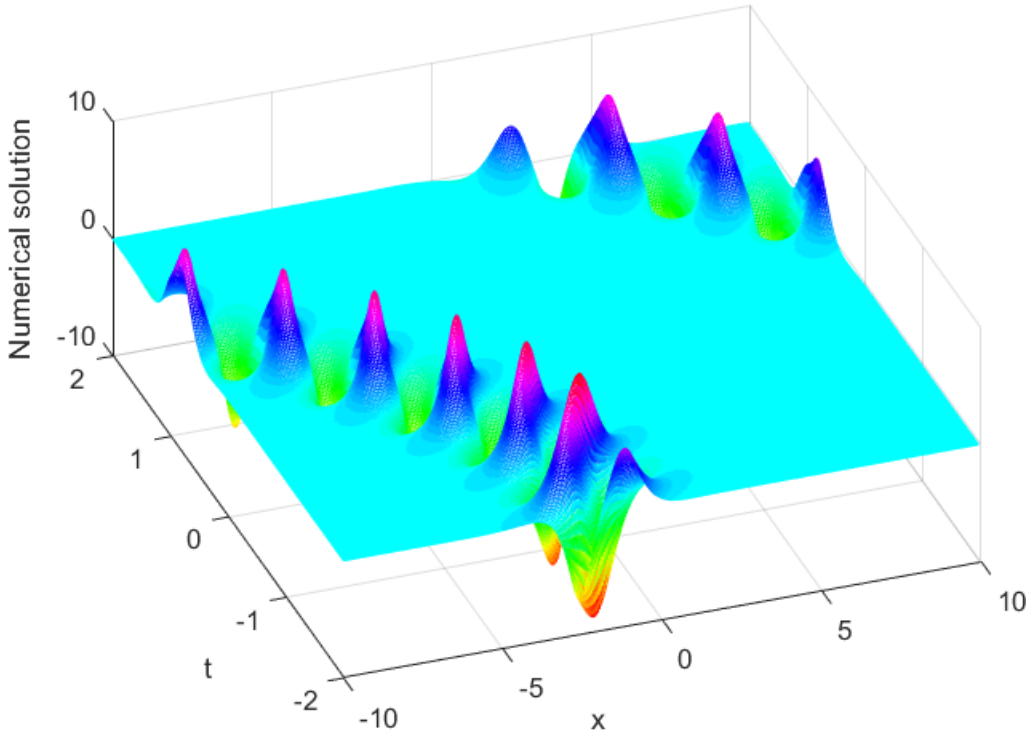

(**a**) $\beta_1 = 0.9995$.

Figure 28. *Cont.*

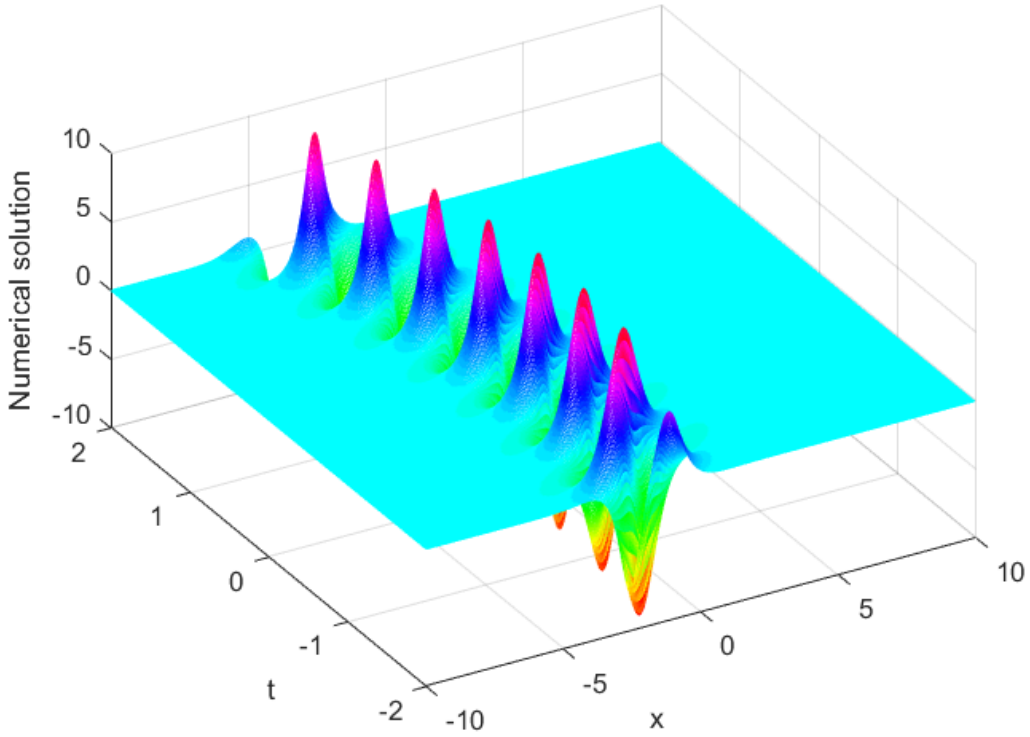

(**b**) $\beta_1 = 0.9999$.

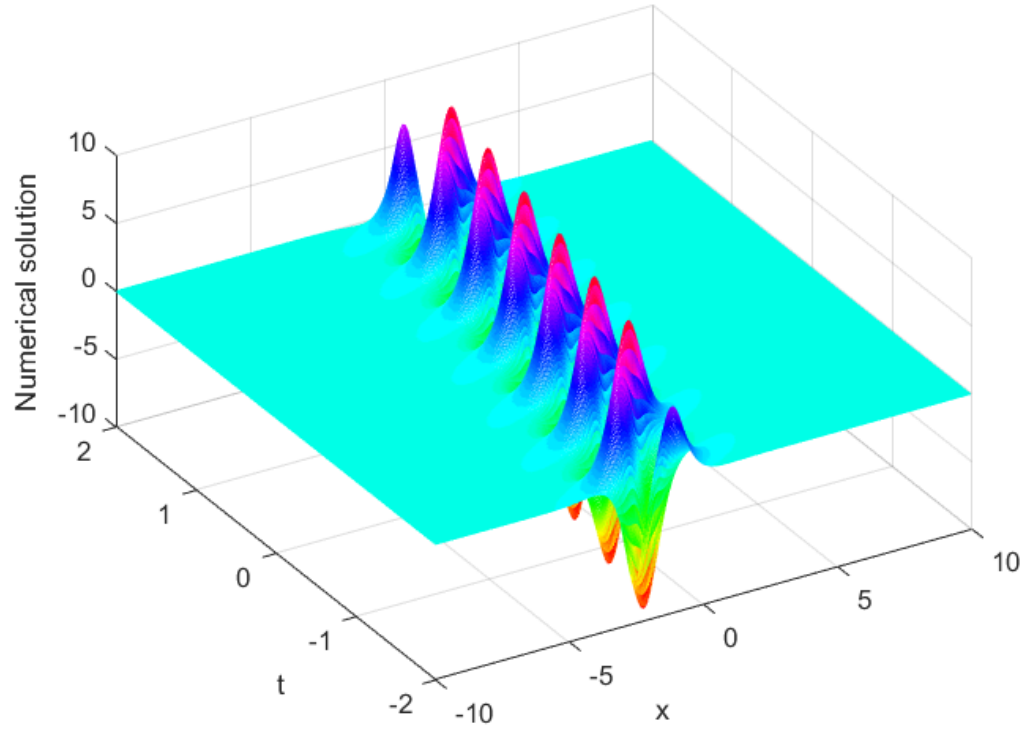

(**c**) $\beta_1 = 0.99999$.

Figure 28. Numerical solutions of vs. at different β_1 , $\alpha_1 = 1, \alpha_2 = 1, k_1 = 1, k_2 = -2$ for Case II.

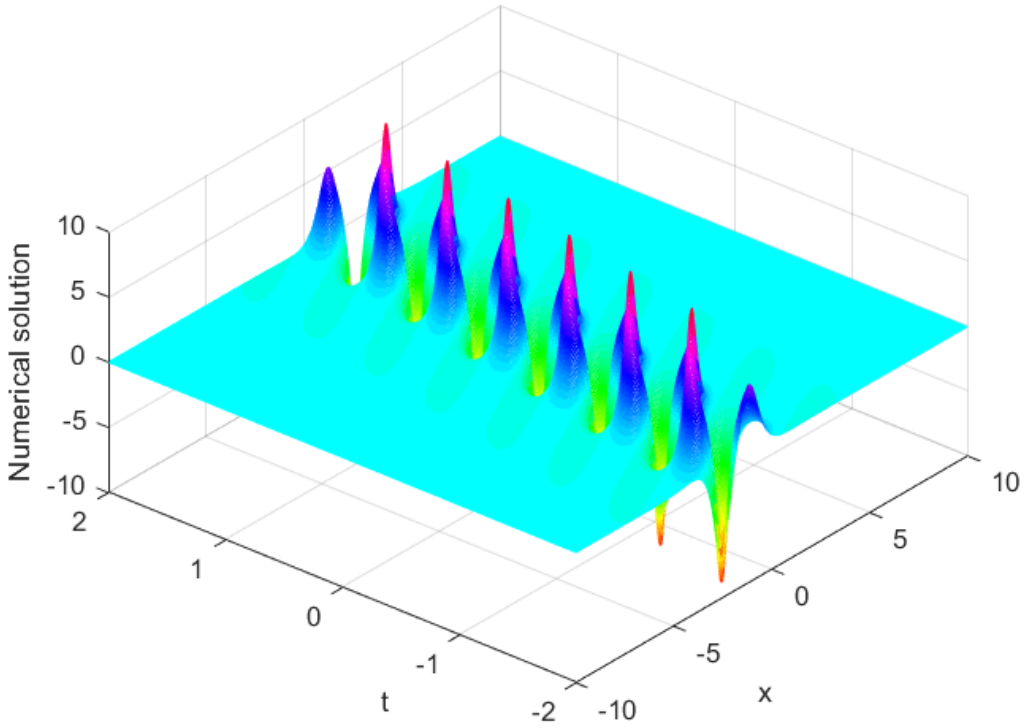

Figure 29. Numerical solution of vs. at $\alpha_1 = 1, \alpha_2 = 1, k_1 = 1, k_2 = -2$ for Case II.

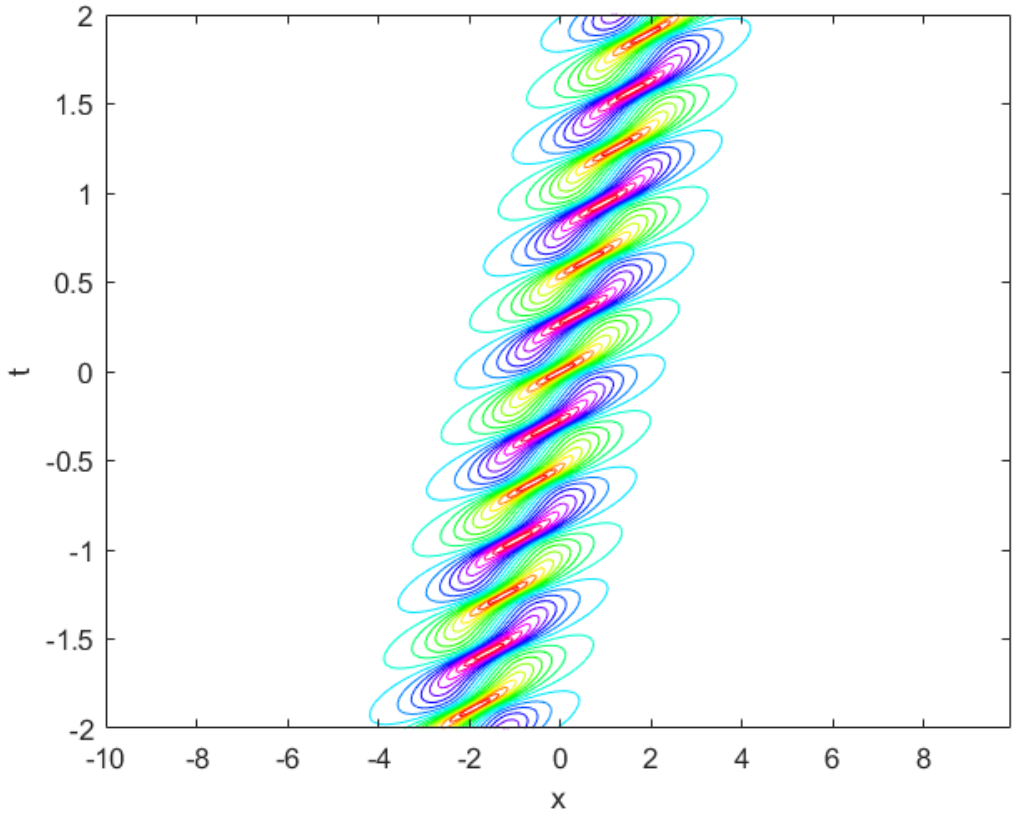

Figure 30. 2D contour plot of vs. at $\alpha_1 = 1, \alpha_2 = 1, k_1 = 1, k_2 = -2$ for Case II.

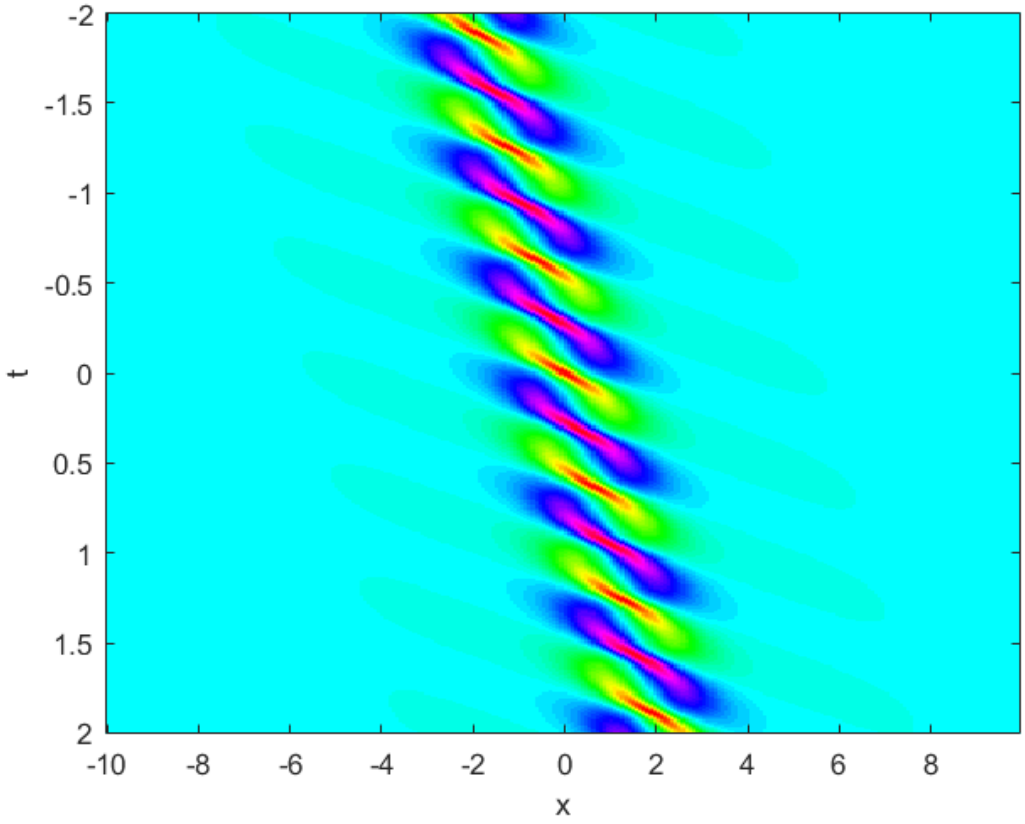

Figure 31. 2D density plot of vs. at $\alpha_1 = 1, \alpha_2 = 1, k_1 = 1, k_2 = -2$ for Example 3.

Through Example 3, we can obtain that if β_1 tends to 1, the numerical solution of the spatial fractional mKdV equation tends to the analytical solution of Equation (6); in addition, the numerical solution of the spatial fractional mKdV equation is very sensitive to a change in β_1.

4. Conclusions

In this manuscript, we study the influence of β_1, β_2 on the numerical solutions of the spatial fractional vcKdV equation. Comparisons are made between the present method and others methods; it can be easily seen that our method has low computational complexity and higher precision. Through Examples 1–3, we know that if β_1, β_2 tends to 1, the numerical solution of the spatial fractional vcKdV equation tends to the analytical solution of the original equation. Through Example 3, the solutions of the space fractional KdV equation are very sensitive to a change in β_1, β_2. From Example 2, we can find that a change in β_1 and β_2 has a minimal effect on the shape of a periodic depression soliton. These results are consistent with the numerical simulation of other scholars [24,27,32].

All computations are performed by the MatlabR2017b software.

Author Contributions: Conceptualization, Y.-L.W.; methodology and software, Y.-L.W. and C.H.; data curation, formal analysis and funding acquisition, Y.-L.W.; writing-original draft and writing-review and editing, Y.-L.W. and C.H. All authors have read and agreed to the published version of the manuscript.

Funding: This paper is supported by the Natural Science Foundation of Inner Mongolia [2021MS01009] and the National Natural Science Foundation of China [11361037].

Institutional Review Board Statement: Not applicable.

Informed Consent Statement: Not applicable.

Data Availability Statement: The data used to support the findings of this study are available from the corresponding author upon request.

Acknowledgments: The authors thank the reviewers for their valuable suggestions, which greatly improved the quality of the paper.

Conflicts of Interest: The authors declare no conflict of interest.

References

1. Korteweg, D.J.; Vries, G.D. On the change of form of long waves advancing in a rectangular canal and a new type of long stationary waves. *Philos. Mag.* **2011**, *39*, 422–443. [CrossRef]
2. Ma, W.X. Linear superposition of Wronskian rational solutions to the KdV equation. *Commun. Theor. Phys.* **2021**, *73*, 5. [CrossRef]
3. Lü, X.; Ma, W.X. Solitary waves with the Madelung fluid description: A generalized derivative nonlinear Schrödinger equation. *Commun. Nonlinear Sci.* **2016**, *31*, 40–46. [CrossRef]
4. Wang, G.W. Symmetry analysis, analytical solutions and conservation laws of a generalized KdV-Burgers-Kuramoto equation and its fractional version. *Fractals* **2021**, *29*, 2150101. [CrossRef]
5. Wang, G.W.; Liu, Y.X.; Wu, Y.B. Symmetry analysis for a seventh-order generalized KdV equation and its fractional version in fluid mechanics. *Fractals* **2020**, *28*, 2050044. [CrossRef]
6. Wang, G.W.; Liu, X.Q.; Zhang, Y. Y. Lie symmetry analysis to the time fractional generalized fifth-order KdV equation. *Commun. Nonlinear Sci.* **2013**, *18*, 2321–2326. [CrossRef]
7. Qin, Y.; Gao, Y.T.; Xin, Y. Bell Polynomial Approach and N-Soliton Solutions for a Coupled KdV-mKdV System. *Commun. Theor. Phys.* **2012**, *58*, 2321–2326. [CrossRef]
8. Chen, S.J.; Lü, X.; Tang, X.F. Novel evolutionary behaviors of the mixed solutions to a generalized Burgers equation with variable coefficients. *Commun. Nonlinear Sci.* **2021**, *95*, 105628. [CrossRef]
9. Yan, J.; Shu, C.W. A Local Discontinuous Galerkin Method for KdV Type Equations. *SIAM J. Numer. Anal.* **2002**, *10*, 769–791. [CrossRef]
10. Jackaman, J.; Papamikos, G.; Pryer, T. The design of conservative finite element discretizations for the vectorial modified KdV equation. *Appl. Numer. Math.* **2019**, *137*, 230–251. [CrossRef]
11. Brugnano, L.; Gurioli, G.; Sun, Y. Energy-conserving Hamiltonian Boundary Value Methods for the numerical solution of the Korteweg-de Vries equation. *J. Comput. Appl. Math.* **2018**, *351*, 117–135. [CrossRef]
12. Geyer, A.; Quirchmayr, R. Shallow water equations for equatorial tsunami waves. *Philos. Trans. R. Soc. A* **2018**, *376*, 20170100. [CrossRef]
13. El-Shamy, E.F. Dust ion acoustic solitary waves in a hot magnetized dusty plasma with charge fluctuations. *Chaos Solitons Fractals* **2005**, *25*, 665–674. [CrossRef]
14. Smyth, N.F.; Worthy, A.L. Solitary wave evolution for mKdV equations. *Wave Motion* **1995**, *21*, 263–275. [CrossRef]
15. Kundu, A. Exact bethe ansatz solution of nonultralocal quantum mKdV model. *Mod. Phys. Lett. A* **1995**, *10*, 2955–2966. [CrossRef]
16. Vaneeva, O.; Kuriksha, O.; Sophocleous, C. Enhanced group classification of Gardner equations with time-dependent coefficients. *Commun. Nonlinear Sci.* **2015**, *22*, 1243–1251. [CrossRef]
17. Gottlieb, D.; Orszag, S.A. *Numerical Analysis of Spectral Methods: Theory and Application*; Society for Industrial & Applied Mathematics: Philadelphia, PA, USA, 1977.
18. Trefethen, L.N. *Spectral Methods in MATLAB*; Society for Industrial & Applied Mathematics: Philadelphia, PA, USA, 2000.
19. Boyd, J.P. *Chebyshev and Fourier Spectral Methods*; Dover Publications: Mineola, NY, USA, 2001.
20. Cooley, J.W.; Tukey, J.W. An algorithm for the machine calculation of complex fourier series. *Math. Comput.* **1965**, *19*, 297–301. [CrossRef]
21. Tian, F.H. Discussion on convergence and stability of standard fourth order Runge–Kutta method. *J. Liaoning Educ. Inst.* **2003**, *20*, 57–58.
22. Han, C.; Wang, Y.L.; Li, Z.Y. Numerical solutions of space fractional variable-coefficient KdV-modified KdV equation by Fourier spectral method. *Fractals* **2021**, *29*, 2150246. [CrossRef]
23. Li, X.Y.; Han, C.; Wang, Y.L. Novel patterns in fractional-in-space nonlinear coupled FitzHugh-Nagumo models with Riesz fractional derivative. *Fractal Fract.* **2022**, *6*, 136. [CrossRef]
24. Han, C.; Wang, Y.L.; Li, Z.Y. A high-precision numerical approach to solving space fractional Gray-Scott model. *Appl. Math. Lett.* **2022**, *125*, 107759. [CrossRef]
25. Frigo, M.; Johnson, S.G. FFTW: An Adaptive Software Architecture for the FFT. In Proceedings of the International Conference on Acoustics, Speech & Signal Processing, Seattle, WA, USA, 15 May 1998; pp. 1381–1384.
26. Kong, D.; Xu, Y.; Zheng, Z. A hybrid numerical method for the KdV equation by finite difference and sinc collocation method. *Appl. Math. Comput.* **2019**, *355*, 61–72. [CrossRef]
27. Aksan, E.N.; Zde, A. Numerical solution of Korteweg-de Vries equation by Galerkin B-spline finite element method. *Appl. Math. Comput.* **2006**, *175*, 1256–1265. [CrossRef]
28. Hao, S.Y.; Xie, S.S.; Yi, S.C. The Galerkin method for the kdv equation using a new basis of smooth piecewise cubic polynomials. *Appl. Math. Comput.* **2012**, *218*, 8659–8671. [CrossRef]

29. ÖZer, S.; Kutluay, S. An analytical-numerical method for solving the Korteweg-de Vries equation. *Appl. Math. Comput.* **2005**, *164*, 789–797. [CrossRef]
30. Kutluay, S.; Bahadir, A.R.; Zde, A. A small time solutions for the Korteweg-de Vries equation. *Appl. Math. Comput.* **2000**, *107*, 203–210. [CrossRef]
31. Wang, P.; Tian, B.; Liu, W.J. Interactions of breathers and solitons of a generalized variable-coefficient Korteweg-de Vries-modified Korteweg-de Vries equation with symbolic computation. *Eur. Phys. J. D* **2012**, *66*, 233. [CrossRef]
32. Lan, Z.Z.; Hu, W.Q.; Guo, B.L. General propagation lattice Boltzmann model for a variable-coefficient compound KdV-Burgers equation. *Appl. Math. Model.* **2019**, *73*, 695–714. [CrossRef]
33. Xi, G.Z. Breather solution to mKdV equation by using variables Separation method. *J. Hexi Univ.* **2009**, *25*, 1–6.